Novel Source Apportionment Methodologies for Secondary $PM_{2.5}$ during Extreme Wintertime Meteorological Conditions in the Western U.S.

Cam M. Phelan[1], Abiola S. Lawal[1†], Kamaljeet Kaur[2], Jenna Krall[3], Kerry E. Kelly[2], Heather A. Holmes[2], and Cesunica E. Ivey[1]*

[1] Department of Civil and Environmental Engineering, University of California Berkeley, Berkeley, CA 94720 USA

[2] Department of Chemical Engineering, University of Utah, Salt Lake City, UT, 84112 USA

[3] Department of Global and Community Health, George Mason University, Fairfax, VA, 22030 USA

*Corresponding Author, iveyc@berkeley.edu

[†]Now at School of Civil and Environmental Engineering, University of Connecticut, Storrs, CT 06269

This article is currently under review in *ACS ES&T Air*

Abstract

Traditional receptor-oriented source apportionment methods, such as positive matrix factorization and chemical mass balance, rely on vector-component analyses of robust observational records or pre-determined source fingerprints, respectively. These methods may struggle to resolve sources that are similar in composition due to source fingerprint collinearity. It is important to isolate contributions with high source specificity to guide mitigation during extreme pollution events. This work explores source apportionment techniques that permit the estimation of contributions from 19 sources during January 2016 in 11 western U.S. cities during cold air pool events. Two apportionment techniques were employed within the Community Multiscale Air Quality model to quantify contributions to 23 speciated $PM_{2.5}$ components: decoupled direct method (DDM) and integrated source apportionment model (ISAM). Source contributions from both DDM and ISAM were used to numerically optimize existing source fingerprints for subsequent use in receptor models, with the goal of using observational nudging to improve location-specific congruence while improving estimations of secondary $PM_{2.5}$. Optimization increased the representation of secondary $PM_{2.5}$ mass by 5.62 to 20.1% on average. Further, when considering California-specific fuel composition for gasoline and diesel combustion fingerprints, diesel profiles exhibited the largest changes after numerical optimization. These analyses highlight the need for localized source fingerprints for apportionment, especially for analyses during extreme air pollution episodes.

1 Introduction

Attribution of fine particulate matter ($PM_{2.5}$) concentrations is increasingly important due to the 2024 tightening of the National Ambient Air Quality Standard (U.S. EPA) for annual $PM_{2.5}$ from 12 μg m^{-3} (2012) to 9 μg m^{-3}.[1] With this new standard comes a greater sensitivity of design value concentrations to changes in emissions.[2,3] With this motivation, the development of methods for better quantification of source contributions to $PM_{2.5}$ becomes more important, especially in regions of the U.S. which are at risk of being in non-attainment for the annual or 24-hour standards and which have large contributions of secondary species to total $PM_{2.5}$.[2]

Moreover, receptor models are empirically driven mass balance approaches for estimating source contributions to ambient $PM_{2.5}$ concentrations.6/14/2026 8:25:00 PM Therefore, receptor models will be particularly useful for carrying out computationally efficient analyses of the response of ambient $PM_{2.5}$ concentrations to changes in key emissions sectors for the purposes of NAAQS compliance. The two principal approaches to receptor model structure, chemical mass balance (CMB) and positive matrix factorization (PMF), both seek to apportion pollution at a receptor by solving for a mass conservation equation.[4] The CMB method requires *a priori* information about the number and composition of all sources, while PMF resolves its source attribution as factor loadings derived from the factor analysis of receptor measurements.[4] Receptor models have also been extensively used to generate multi-decadal time series of $PM_{2.5}$ source

impacts to drive epidemiological studies that seek to connect various health end points to source-specific, population-weighted exposures.[5] This approach is computationally efficient compared to typical chemical transport model applications but is limited by several issues. Some of the issues cited in these studies include limited source diversity,[6,7] collinearity issues for resolving sources with similar fingerprints,[4,8] and the inability to directly link the secondary contribution from primary sources to source impacts.[6] A preceding study has investigated the use of inverse modeling approaches, specifically nonlinear optimization to take secondary transformation into consideration for the development of $PM_{2.5}$ source profiles.[6]

In a wintertime case study for Salt Lake City, Utah (U.S.), optimized profiles were used in a CMB application to evaluate the ability to resolve elevated $PM_{2.5}$ levels during stagnant conditions known as persistent cold air pool (PCAP) events.[7] PCAPs are prevalent in the western U.S. during wintertime, oftentimes forming as a result of synoptic-scale, high-pressure ridges that stall over mountainous regions.[9,10] Highly populated regions within mountain valleys are susceptible to PCAPs, where stable atmospheric layers and stagnant conditions inhibit mixing and transport out of the air basin. These events are characterized by reduced planetary boundary layer heights, wind speeds and air temperatures, as well as increased relative humidity and valley heat deficit values.[9,11,12] The Salt Lake Valley, in particular, is prone to PCAPs in the winter, and the resulting increase in $PM_{2.5}$ concentrations during this period has placed the region in serious nonattainment of the 24 hour average standard (35 $\mu g\ m^{-3}$ as of 2006).[9,13] In the Salt Lake City application, optimization was only applied for trace metals and elemental carbon (EC), incorporating the impact of pollutant transport but not chemical transformation (i.e., atmospheric aging). The study found that gasoline vehicles, combustion of natural gas, and various industrial sources were major sources of $PM_{2.5}$ in the area, with changes in source importance with PCAP event inversions.[7]

The source apportionment method used in this study was a combination of receptor modeling with ambient concentration measurements and emissions sensitivities from a chemical transport model, such as CMAQ. Nonlinear optimization was applied to CMAQ sensitivity products and observed concentration data to generate optimized profiles for CMB analysis. This approach is especially useful as it considers the impacts of transport from the source to the receptor and the secondary formation of aerosols. The incorporation of observed concentrations at the receptor accounts for biases in modeled total and speciated $PM_{2.5}$ concentrations (see Eq. 1,) as well as the inherent uncertainties in both simulations and observations.[6,14] These methods have since been applied in several studies over various spatial domains and used to connect source concentrations to population exposures and health endpoints.[7,15,16]

In this study, we sought to incorporate both transport and chemical transformation within $PM_{2.5}$ source profile optimization by including species that undergo significant secondary transformation, including organic carbon (OC), nitrate (NO_3), ammonium (NH_4), and sulfate (SO_4). We also included additional source categories that predominantly contribute to these secondary aerosol species: agriculture/livestock activities and biogenics. These two sources are

not commonly represented in receptor modeling studies, but their secondary impacts on $PM_{2.5}$ can be captured with this profile development method.[17] This study also compares the results of source profile optimization using different CMAQ modules as source-species sensitivity input data. We also generated numerically optimized profiles with these outputs for multiple days in the study period and can compare averaged profiles for PCAP and non-PCAP wintertime conditions in ten sites across the western U.S., including California's Central Valley. Given the more stringent regulations for fuel composition and vehicle emission controls in California, we also generated optimized profiles at these sites with CMAQ-ISAM data using an updated seed profile based on EPA SPECIATE observations of on road diesel and gasoline mobile source emissions. The comparison of these methods serves as a sensitivity analysis for the impact of seed profile choice on final source profiles.

2 Methods

2.1 Surface Observations

Speciated $PM_{2.5}$ observational data were obtained from the Chemical Speciation Network (CSN) for all available days in January 2016. Quality assurance steps were performed in accordance with Kaur et al. (2024) to account for analytical changes over time for carbonaceous (OC and elemental carbon (EC)) and ionic species (NO_3, NH_4, and SO_4).[18] The study locations, each collocated with a CSN monitor, were Bakersfield, California (BAK); Boise, Idaho (BOI); Bountiful, Utah (BOU); Denver, Colorado (DEN); Fresno, California (FNO); Hawthorne, Salt Lake City, Utah (HAW); Las Vegas, Nevada (LAS); Modesto, California (MOD); Reno, Nevada (REN); Sacramento, California (SAC); and Visalia, California (VIS) (Figure 1). See Supplemental Information for additional metadata on each site (Table S-3).

Previous work has shown that prevalent sources in the study locations include on and off-road mobile source emissions (all sites), agriculture activities (sites excluding Las Vegas), resuspended dust (all sites), and industrial oil and metals activities (especially at Bakersfield, Bountiful, and Hawthorne).[19] Some notable sources in the Salt Lake Valley in Utah include the drying Great Salt Lake and the collocated US Magnesium plant, which has been linked to emissions of Cl, HCl, and Br in several studies.[19–21] Significant sources of SO_2 during the study period include the Boise Amalgamated Sugar plant and the Reid Gardner power generation plant in Las Vegas (which ceased operations in 2019).[19]

For the sites in Boise, Bountiful, Denver, Hawthorne, Las Vegas, and Reno we used twice-daily (0:00 and 12:00 UTC) radiosonde observations from the University of Wyoming UpperAir data repository to determine whether a particular day (site-specific) was a PCAP event using methods from previous work.[22] This approach yielded one of three results: definite ("strong") CAPs, uncertain ("weak") CAPs, and non-CAPs. Day-by-day data on the results of this analysis may be found in the Supporting Information, Table S-4. The two sites situated on the Wasatch Front in Utah (BOU and HAW, see Figure 1 inset) were deemed close enough together to use the same radiosonde-based PCAP determination at both sites. In Bakersfield, Fresno, Modesto,

Sacramento, and Visalia, this method was implemented with ERA5 reanalysis data in lieu of radiosonde data.[12] In all cases, a PCAP was defined as at least two strong or weak CAP days in a row.

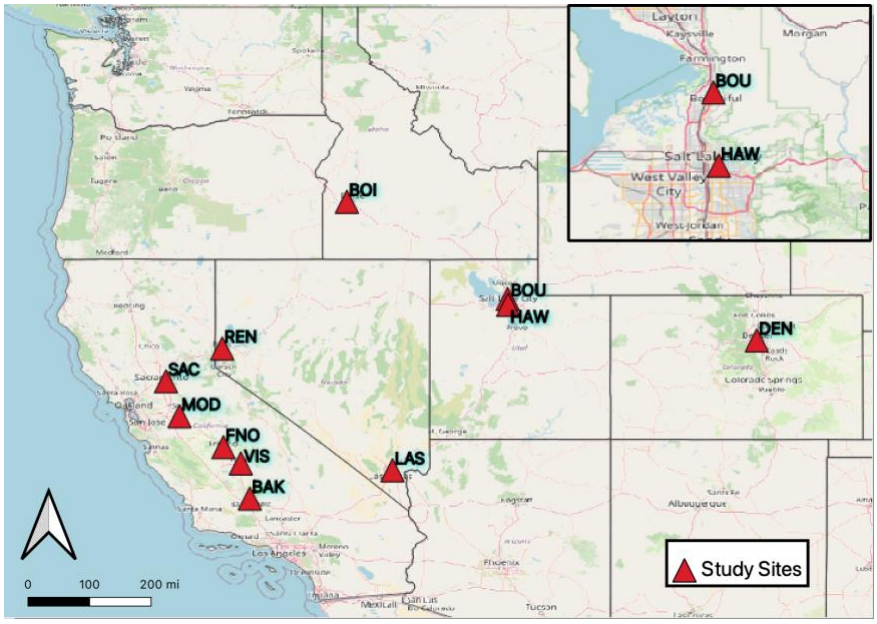

Figure 1 Study locations in the western U.S. at Chemical Speciation Network sites. The inset map highlights the study locations along the Wasatch Front in northern Utah, near Salt Lake City.

2.2 Source Apportionment Modeling and Inputs

$PM_{2.5}$ source impacts for a representative wintertime seven-day period (December 31, 2015 – January 6, 2016) were simulated using the Community Multiscale Air Quality Model with the decoupled direct method (CMAQ-DDM v5.4).[23,24] A longer simulation period (December 31, 2015 – January 31, 2016) was possible with CMAQ's Integrated Source Apportionment Method (ISAM) due to its robustness to numerical instability issues that limited the CMAQ-DDM run to four days. Both the CMAQ-DDM and CMAQ-ISAM simulations used a 10-day spin-up period (21-30 December 2015).

Source impacts are the quantified mass that is attributed specific source groupings. Specifically, source impacts were directly output from CMAQ for the following $PM_{2.5}$ components: OC, EC, NO_3, NH_4, SO_4, Na, Al, Si, Cl, K, Ca, Ti, Mn, and Fe. The sensitivities of unspeciated $PM_{2.5}$ mass from CMAQ were used to derive source impacts for the following components: Cu, Zn, As, Se, Br, Sn, Sb, Ba, and Pb. It is assumed that the derived components represent the majority of unspeciated $PM_{2.5}$ mass, since observations of these species are most often above measurement detection limit.[17] The source impacts for derived species were estimated using seed profiles that were developed with the primary $PM_{2.5}$ emissions reported in Reff et al. (2009) (Table S-1), and 19 source categories were of interest for this study (Figure 2, Table S-2**)**.[25] See the Supplemental Information for a description of each source category (Table S-5). It is

important to note that two source categories (AG and BIO) were specially derived for this application, and details are provided in Section 2.3 that follows.

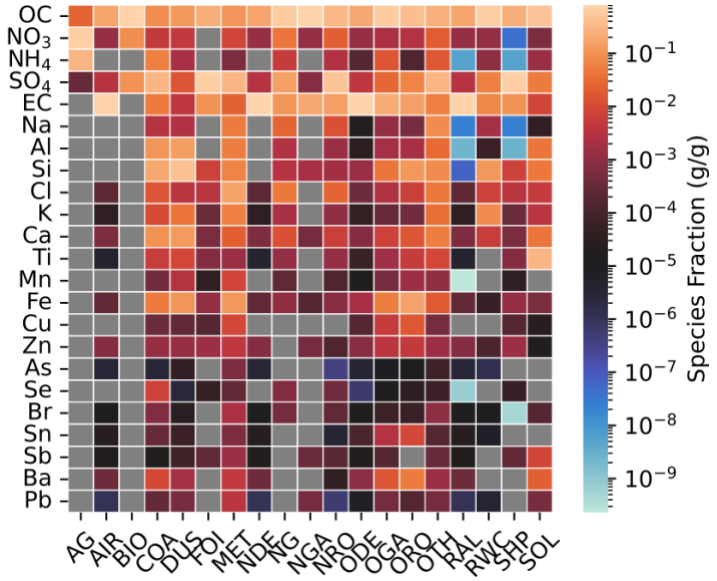

Figure 2 Seed $PM_{2.5}$ source profiles derived from primary $PM_{2.5}$ emissions by Reff et al., with added source profiles for agriculture (AG) and biogenics (BIO). Gray squares indicate that the species is not contributed by the source.

Meteorology and emissions inputs were generated offline using the Weather Research and Forecasting (WRF) model version 4.3.3 and the Sparse Matrix Operator Kernel Emissions (SMOKE) model, respectively. The modeling domain for WRF, SMOKE, and CMAQ-DDM had 12-km horizontal grid spacing, 35 vertical layers, and covered the continental U.S. Science options for WRF and CMAQ are reported in the S.I. (Tables S-6 and S-7). Gridded emissions inputs were generated and separated by source sector using SMOKE, based on the 2017 National Emissions with adjustments for the model year 2016.[26]

To reflect local and state policies and legislation on emissions restrictions, the following processing steps were applied to either emissions inputs or sensitivity outputs. In the case of coal combustion (COA) in California and the Salt Lake Valley, which is banned in practice but is represented in emissions inventories as reported in other studies, we set all sensitivities of $PM_{2.5}$ to coal to zero before optimization.[27–29] Similarly, for Utah sites Bountiful and Hawthorne, all RWC impacts from either CMAQ-DDM or CMAQ-ISAM were set to zero, as local policy in the Salt Lake Valley has banned such activities between November 1 and March 1 every year, supported by studies suggesting that these restrictions drastically improve wintertime air quality in the region.[27,30–32]

2.3 Aged Source Profile Development

In this work, seed $PM_{2.5}$ source profiles were "aged" using a nonlinear optimization approach[6,7] that is designed to increase the congruence of the sum of the source *j* impacts ($SA_{i,j}^{base}$) on $PM_{2.5}$ species *i* and the corresponding ground observations of species *i* (Eq 1):

$$X^2 = \sum_{i=1}^{I}\left(\frac{\left[c_i^{obs}-(\sum_{j=1}^{J} r_{ij} f_{ij}^0 SA_{i,j}^{base})\right]^2}{\sigma_{i,obs}{}^2+\sigma_{i,SA}{}^2}\right) + \alpha\Gamma \sum_{i=1}^{I}\left(\sum_{j=1}^{J}\left[\frac{f_{ij}^0(r_{ij}-1)}{\sigma_{f_{ij}}} * U(f_{ij}^0)\right]^2\right) \quad (1)$$

In Eq. 1, X^2 is the term to be minimized, and r_{ij} is the term to be optimized, which represents an adjustment factor ranging from 0.5 to 2 to be applied to the fractional contributions of sources *j* (J = 19) to species *i* (I = 23). The optimization is applied at one location for one discrete time period (e.g., one day), aligning with the time resolution and availability of the observations. The variable c_i^{obs} is the ground observation of species *i,* and f_{ij}^0 is the seed fractional contribution of source *j* to species *i*. Variables $\sigma_{i,obs}$, $\sigma_{i,SA}$, and $\sigma_{f_{ij}}$ are uncertainties in the ground observations, CMAQ-DDM or CMAQ-ISAM source impacts, and seed fractional contributions of source profiles, respectively. The variable α is a numerical sensitivity term, Γ (0.01) is a weighting variable, and U is a constraining variable. See Supporting Information for additional details on variable descriptions (Text S-1). The aging of profiles is reflected after adjustment (Eq. 1):

$$f_{i,j} = r_{i,j} f_{i,j}^0 \quad (2)$$

In Eq. 2, $f_{i,j}$ is the aged fractional contribution of source *j* to species *i*. The matrix *f* of $f_{i,j}$ for all species *i* and sources j is then normalized such that the contribution of source *j* for all species *i* equals unity (Eqs. 3 and 4) This normalization ensures that all optimized profiles can be compared against each other and that $f_{i,j}$ represents the fraction of species *i* expected from emissions of source *j* in the receptor $PM_{2.5}$.

$$f_{i,j}^{norm} = \sum_{i=1}^{I} f_{i,j}^{norm} = 1 \quad (3)$$

$$f_{i,j}^{norm} = \frac{f_{i,j}}{\sum_{i=1}^{I} f_{i,j}} \quad (4)$$

As stated previously, two source profiles were specially developed for this application. Specifically, profiles for agricultural activities and livestock operations (AG) and biogenics (BIO) were constructed using published literature values.[14] For this study, it is assumed that OC, NO_3, NO_4, and SO_4 are the dominant species within an aged profile. In a preceding study, it was estimated that agriculture/livestock $PM_{2.5}$ comprises 2.48% OC, 67.12% NO_3, 30.27%, and 0.03% SO_4.[14] These values are based on the average CMAQ-DDM impacts for AG at CSN locations in 2006.[14] For the biogenics seed profile, aged aerosol is estimated to comprise 81.1% OC, 9.0% NO_3, and 9.9% SO_4. These values are estimated using molecular weights of organic nitrates and organosulfates in the southeastern U.S.[33] It is worth noting that AG and BIO are sources that are not traditionally reflected within receptor modeling applications given their emissions are the

precursor species to secondary $PM_{2.5}$ and therefore harder to directly represent in an unaged source-receptor relationship. The aged, source-oriented approach applied here facilitates their inclusion in such applications.

Two types of optimized profiles were created with the CMAQ-DDM outputs. The first profiles used unconstrained ("raw") sensitivities that included negative values, which were often found for secondary species such as OC, NO_3, and NH_4. These unconstrained profiles will be referred to as "Raw DDM" profiles in the remainder of this work. The other set of profiles generated with CMAQ-DDM data positively constrained the sensitivity data inputs, which has been implemented in other work to constrain impacts of primary emissions on secondary concentrations in aged sources.[14] The positively constrained profiles will be referred to as "NN DDM" or "Non-Negative DDM" profiles in the following analysis.

2.4 Aged Profile Development Incorporating California Fuel Regulations

California legislation developed between 1993 and 2014 has led to a more stringent gasoline specification (CaRFG) that is the only blend allowed for sale and use within the state. California Air Resources Board (CARB) rules specify that gasoline in the state must, as of Phase 3 of the standard that started in 2011, contain no more than 20 ppm sulfur by mass and no more than 0.80% benzene, 25.0% aromatics, 6.0% olefins, and 1.8-2.2% oxygen by volume.[34] Methyl tertiary butyl ether (MBTE) and all other oxygenates except ethanol are also prohibited in this blend as of December 31, 2003.[34]

Diesel sold within California must not exceed 15 parts per million sulfur by weight (as of 2006) or 10 percent aromatic compounds by volume (as of 1993).[35] This standard applies to all diesel sold in the state for on road or offroad vehicular use, harbor craft, and diesel-electric intrastate locomotives.[26] The standard is not applicable to diesel fuel solely for use in marine vessels or locomotives.[35] Furthermore, CARB has required the use of emissions control devices on diesel vehicles since 2010, including diesel particle filters (DPF) to reduce direct $PM_{2.5}$ emissions and selective catalytic reduction (SCR) systems to reduce NO_x emissions, which change the profile of both primary and secondary $PM_{2.5}$ emissions in California compared to the less stringent federal standards.[19,36–38] The use of these control devices can also add different pollutants into the emissions stream, such as ammonia slip from SCR devices.[37] It should be noted that the fleet of diesel and gasoline vehicles in California has a wide range of vehicle model years and emissions controls which leads to significant differences in emissions profiles across vehicle ages and control device lifetimes.[36,37] Even vehicles with emissions control devices have heavily skewed emissions distributions; one study found that 5% of trucks with SCR contributed 97% of the total NH_3 while in-use on a California freeway.[37]

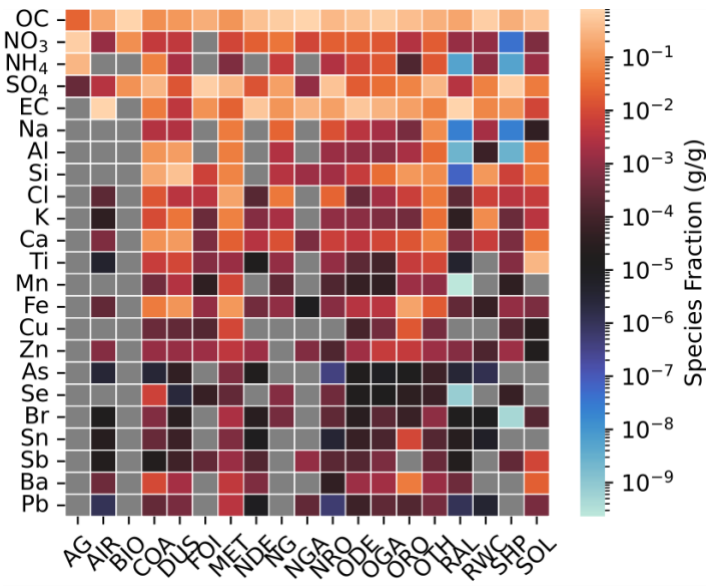

Figure 3 California-specific $PM_{2.5}$ seed profiles based on the standard seed (Figure 2) and modified to reflect California on-road diesel and gasoline emissions profiles from EPA SPECIATE. The only sources that were modified from the standard seed were: NDE, NGA, ODE, and OGA.

To capture the effects of these state-specific differences in optimization, we created a new seed profile based on the profile ("standard seed" elsewhere in this paper) discussed above and shown in Figure 2. Every source except NDE, NGA, ODE, and OGA remained identical to the standard seed profile. On-road sources (ODE and OGA) were replaced with an average of California on-road profiles, using 48 gasoline profiles and 141 diesel profiles with emissions controls found in EPA SPECIATE v5.3. Non-road sources (NDE and NGA) were updated using the ratio of the SPECIATE profile to the standard seed for the corresponding fuel type (i.e., the standard NGA profile was multiplied by the ratio of updated OGA to standard OGA to yield the updated NGA). Figure 3 shows this updated seed profile ("CA seed" elsewhere in this work) for all $PM_{2.5}$ sources and species. The updated CA seed was then used to generate optimized profiles for ISAM sensitivities at Bakersfield, Fresno, Modesto, Sacramento, and Visalia over January 2016 using the same methods as in Section 2.3, producing optimized profiles that will be referred to as "CA ISAM" profiles in the following sections for each of the days with CSN observations.

3 Results and Discussion

3.1 Western U.S. Wintertime Observations of Speciated $PM_{2.5}$

Speciated $PM_{2.5}$ concentrations were obtained from the CSN network.[18] The correction method used in Kaur et al. (2024) to account for analytical changes over time for carbonaceous (OC and elemental carbon (EC)) and ionic species (NO_3, NH_4, and SO_4) was applied to the data at all sites, available in Table S-8 in the SI.[18] Figure 4, below, shows these corrected observations of speciated

$PM_{2.5}$ concentrations in January 2016, grouped by major constituent types. "Other Metals" included Ti, Cu, Zn, Fe, Mn, Pb, and Sn. "Trace Elements" included Se, Cl, Br, As, and Sb.

Most of the observed mass in the study sites is composed of OC, EC, NO_3, SO_4, and NH_4, with total $PM_{2.5}$ concentrations reaching over 40 μg m^{-3} at Bakersfield, CA. Previous studies have indicated that ammonium and nitrate $PM_{2.5}$ concentrations are elevated during PCAP episodes along the Wasatch Front, often comprising the majority of observed mass.[13,32] For example, sites with PCAPs on January 1 (Bakersfield, Boise, Bountiful, Denver, Hawthorne, Las Vegas, and Reno) had mean ammonium and nitrate concentrations of 1.83 and 6.43 μg m^{-3} respectively, which on average contributed to 47.1% of total $PM_{2.5}$ mass. In contrast, non-PCAP sites on January 1 (Fresno, Modesto, Sacramento, and Visalia) had average ammonium and nitrate concentrations of 2.08 and 6.81 μg m^{-3} respectively, an average of 39.5% of total $PM_{2.5}$ at these sites.

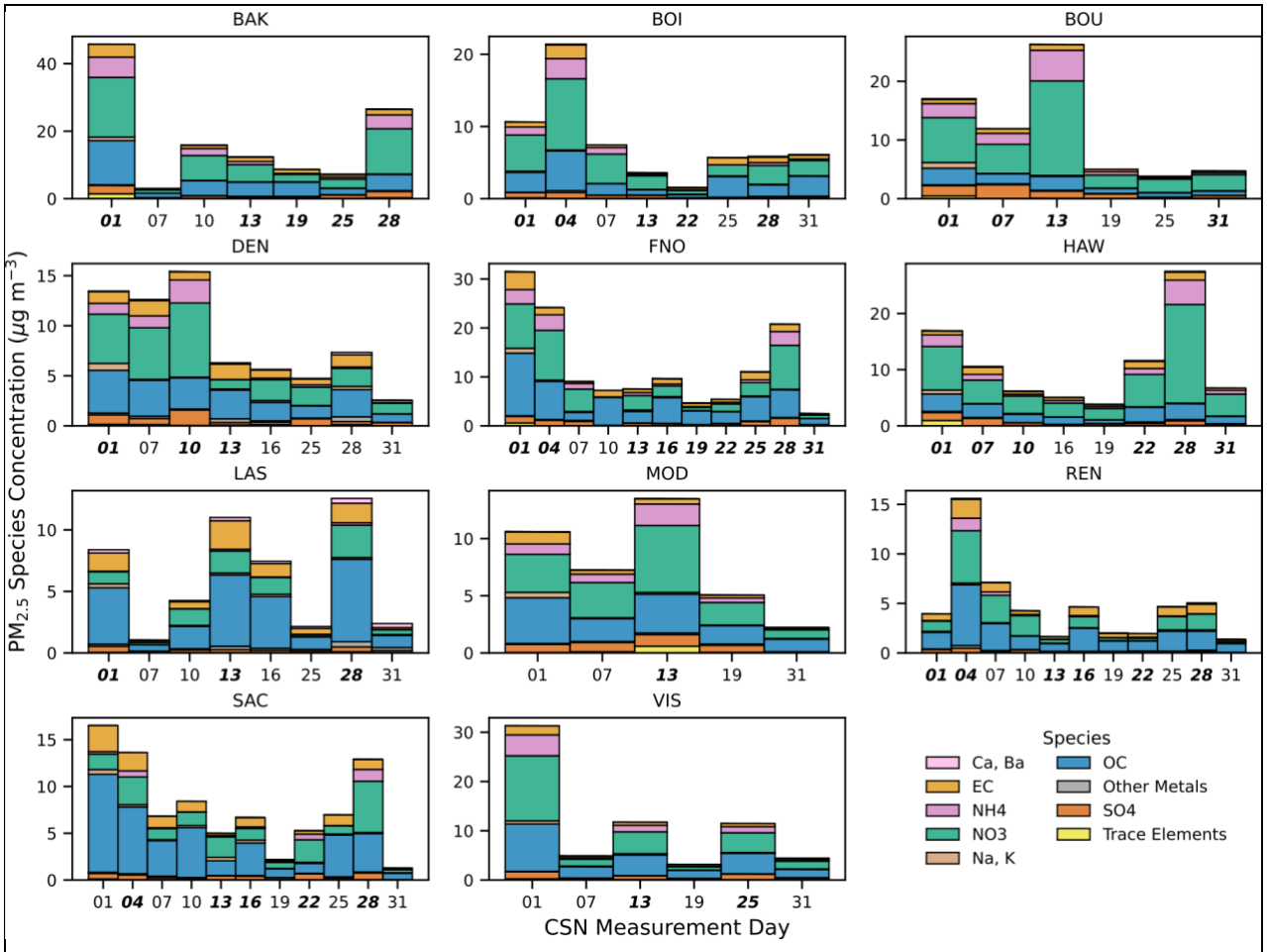

Figure 4 CSN observations of chemically speciated $PM_{2.5}$ at study locations in January 2016. Tabulated, full measurements are in the S.I. in Table S-8. Bars with bold, oblique tick labels indicate that a measurement was made during a PCAP.

For profiles developed using CMAQ-ISAM, we were able to use all CSN observations from the month of January, allowing for comparison of PCAP and non-PCAP source profiles and

sensitivities at the same sites. Figure 5 compares PCAP and non-PCAP concentrations and compositions of $PM_{2.5}$ at the remaining ten sites.

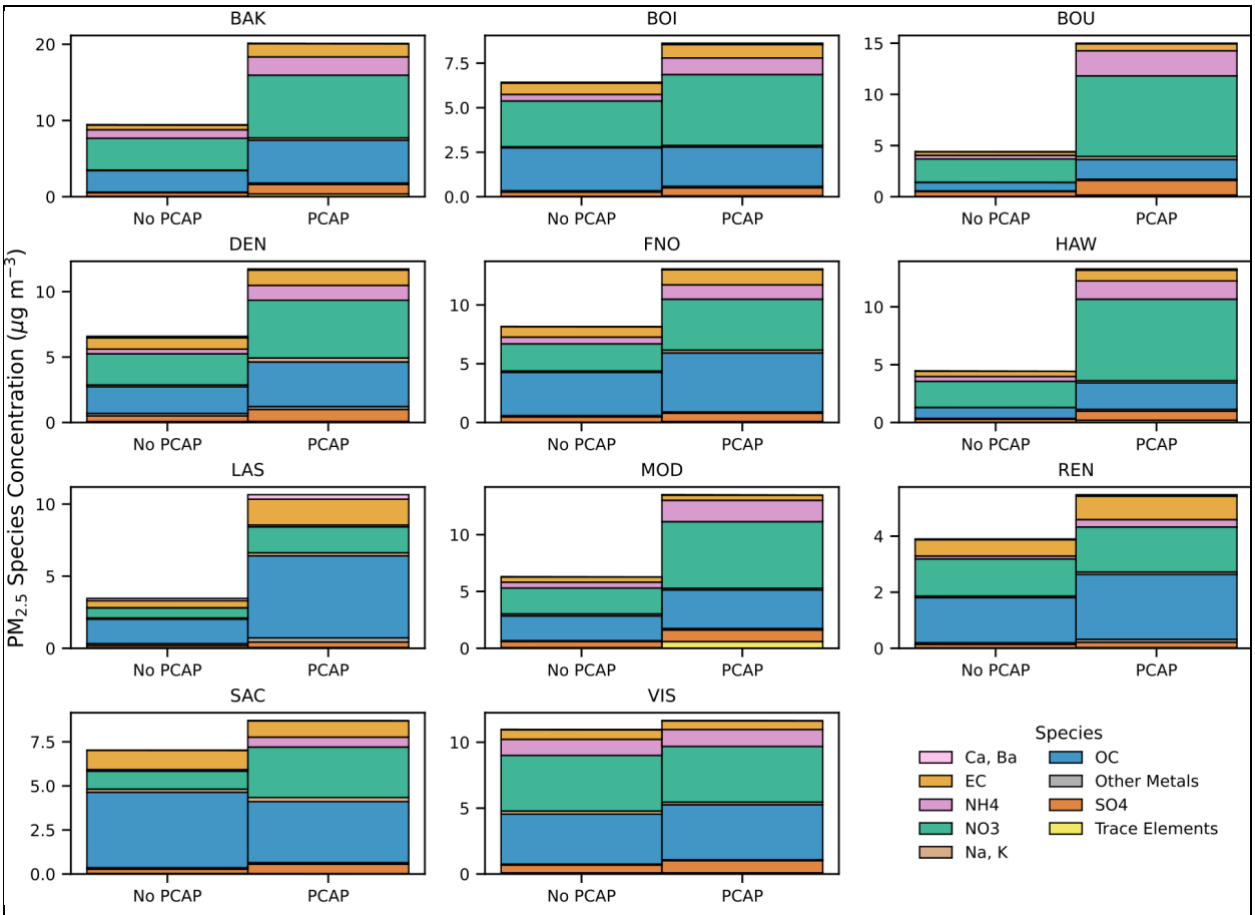

Figure 5 Averaged January 2016 observations of chemically speciated $PM_{2.5}$ excluding (left bars) and during (right bars) PCAPs at the study sites.

At all ten sites, total $PM_{2.5}$ concentrations increased by 1.66 to 18.87 μg m^{-3} during PCAPs, or a 17 to 300% increase from non-PCAP concentrations. On average, concentrations of all $PM_{2.5}$ species increased by 24% during PCAPs, with nitrate and ammonium increasing by 3.11 μg m^{-3} (150%) and 1.03 μg m^{-3} (300%) respectively. The contribution of nitrate to total $PM_{2.5}$ increased by 0.98 to 13.8 percentage points at eight of the ten sites, with Las Vegas and Reno nitrate contributions decreasing by 2.43 and 4.97 percentage points, respectively. In those cases, however, the PCAP nitrate mass still increased. On the other hand, ammonium contributions to total $PM_{2.5}$ mass increased during PCAPs at all ten sites, with the increase in contribution ranging from 0.65 to 8.4 percentage points. The other major species, SO_4, OC, and EC, had mixed responses to PCAP conditions. Sulfate composition of total $PM_{2.5}$ changed by -2.96 percentage points (at Bakersfield) to +1.51 percentage points (Denver). OC composition only increased at LAS and REN, where nitrate contributions dropped during PCAPs. EC compositions decreased by up to 4.15 percentage points during PCAPs but did increase by 2.98 and 0.29 percentage points at LAS and REN. This

behavior at Las Vegas and Reno could reflect differences in climatology at those sites or the differences in local and state level air pollution control policies. In general, however, we do observe an increase in secondary $PM_{2.5}$ concentrations and contributions to total $PM_{2.5}$ during PCAPs in the study period, aligning with prior observations from the literature.[13,32]

3.2 Source Impact Trends in CMAQ-DDM and CMAQ-ISAM

Sensitivities derived from CMAQ-DDM and CMAQ-ISAM at each site are presented here. Sensitivity of a species to a source sector (in units of μg m^{-3}) can be either positive or negative when using the DDM feature in CMAQ.[24] This behavior, while nonintuitive, reflects the nonlinearity of aerosol thermodynamics, as the addition of certain precursor species to a system can decrease the proportion of other speciated mass in the aerosol phase, such as the sulfate-nitrate-ammonium-water system.[39] However, in some cases, positively constraining the sensitivities of speciated $PM_{2.5}$ can better capture the impacts of emissions on secondary $PM_{2.5}$ species.[14] Figure 6, below, shows CMAQ-DDM and CMAQ-ISAM source impacts for a site in the Salt Lake Valley on January 1, and the same information is available for all sites in the Supplemental Information (Figures S-1 to S-11).

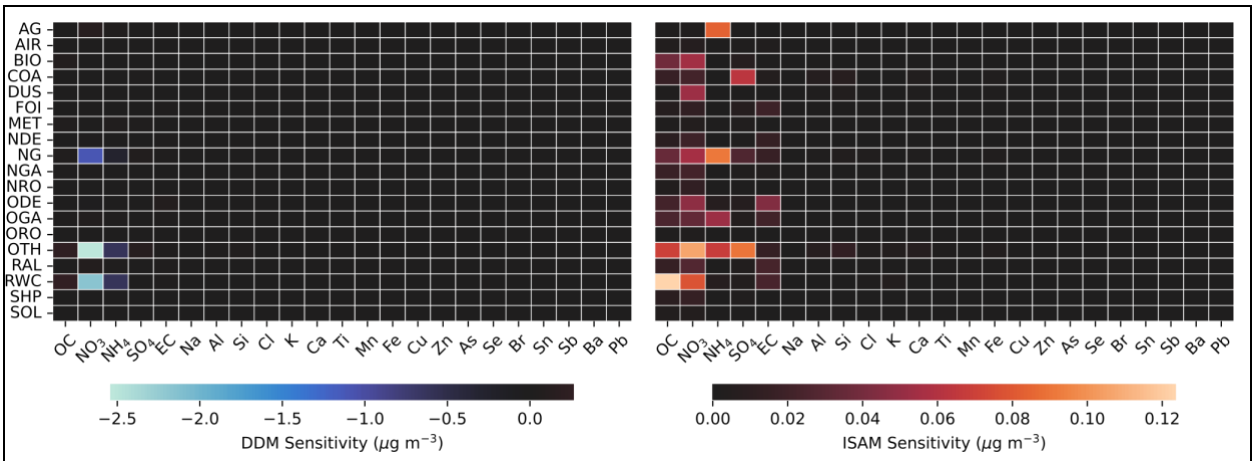

Figure 6 CMAQ-DDM and CMAQ-ISAM sensitivities in Bountiful, UT on January 1, 2016. Sensitivities for Cu through Pb were derived from unspeciated $PM_{2.5}$ outputs in both models.

When comparing negative DDM sensitivities to the corresponding ISAM values, there is an inverse relationship where the greater the negative sensitivity was for DDM, the ISAM apportioned concentration was higher. These negative sensitivities in DDM were frequently associated with secondary species, especially nitrate and ammonium. Negative sensitivities for sulfate and OC were smaller but still existed.

3.3 Source Profile Optimization Results

The outputs of DDM and ISAM are not quite comparable given the methods used in each model; however, the optimized profiles using said outputs can be directly compared for the allocation of speciated mass to different sources. Figure 7 compares the products of nonlinear optimization at

Bountiful, UT, a site in the Salt Lake Valley close to Salt Lake City. The profiles are normalized such that the sum of species contributions in each source total 1, with units being grams of speciated $PM_{2.5}$ per gram emitted by the source (see Eqs. 3 and 4).

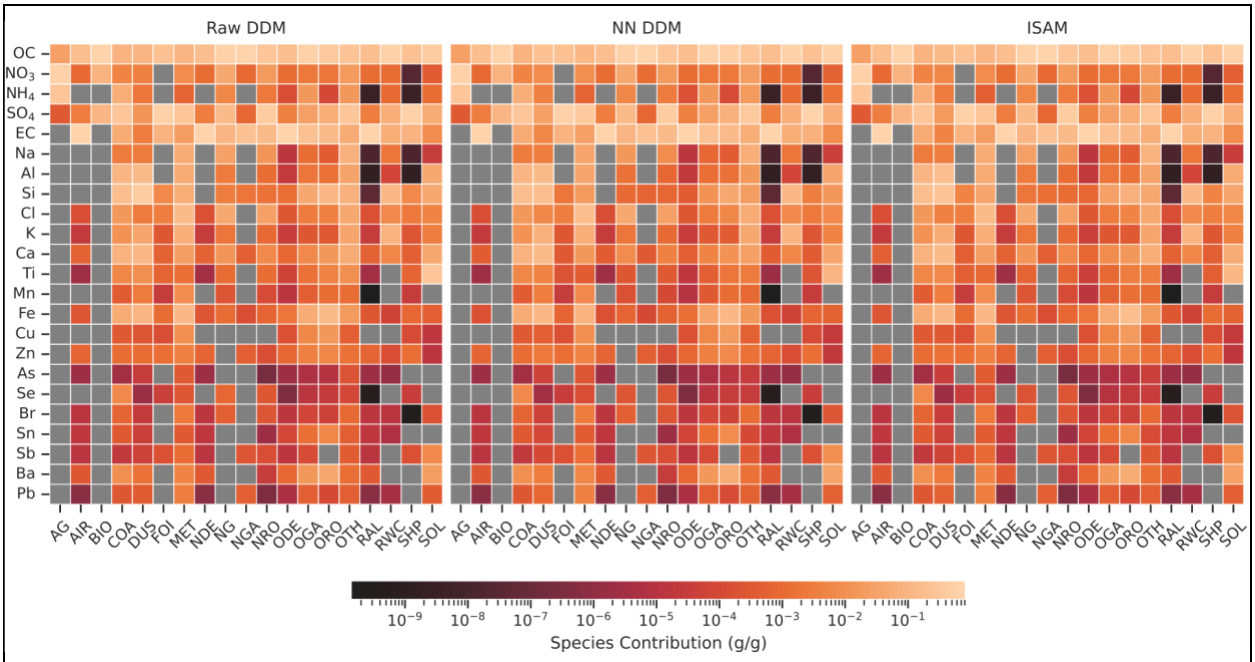

Figure 7 Optimized source profiles for Bountiful, UT on January 1, 2016 using raw DDM outputs, positively constrained DDM outputs, and ISAM outputs and the standard seed.

The impacts to optimized profiles of constraining sensitivities of secondary species, especially nitrate and ammonium, are not immediately obvious, as many of the optimized sources are composed of secondary $PM_{2.5}$ species and EC. The impacts on tracer species, however, may have greater implications for the use of optimized profiles. CMB source apportionment cannot be run with collinear sources that have similar compositions, so the optimization of trace species in source profiles may increase CMB performance in mass closure and error minimization.

Figure 8 shows the cosine similarity between the optimized profiles and the seed profile on an individual source basis. Cosine similarity indicates the difference in relative importance of component species within a source, with zero indicating large, important differences in species contributions and one indicating that there are no notable species-level differences. The lowest similarities are in the profiles without negative sensitivities as inputs: non-negative DDM and ISAM. However, the raw DDM profile does have some sources with low similarity to the standard seed: COA, DUS, and MET. These sources also have low cosine similarity between the other optimized profiles and the standard seed.

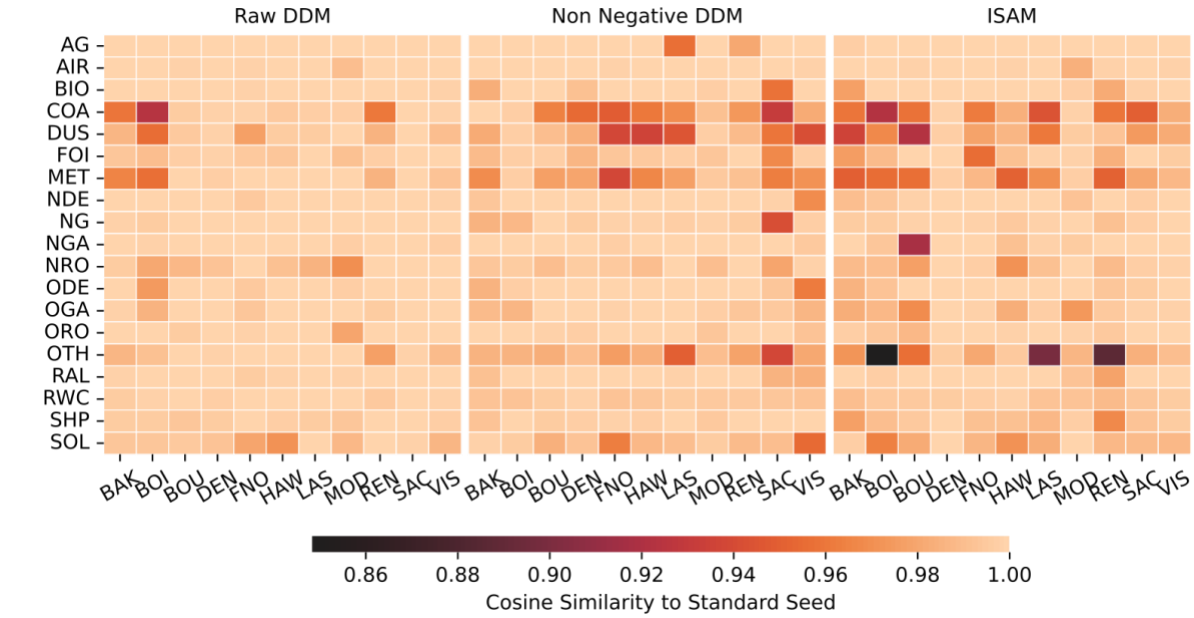

Figure 8 Cosine similarity between optimized source profiles and the standard seed profile (Figure 2) at all sites. A value of 1 indicates a perfect agreement in the vectors of species contributions in a source profile. Values indicating good agreement range from 0.95 to 1.

However, the smallest cosine similarities can be found between ISAM and the seed in the OTH source, which acts as a catch-all for any source in the CMAQ inputs that does not correspond to one of the other 18 source categories (explained in Table S-5). Sources with relatively small departures from the standard seed include AG, AIR, BIO, ORO, RAL, and RWC. The sites with the most departures of optimized profiles from the seed were BOI, BOU, and REN, all of which were experiencing a PCAP during the modeling period that was used for optimization.

In section 3.2, we found that the sources with the largest differences in sensitivity were NG, AG, DUS, and OTH while the species with the most differences were nitrate, ammonium, and some trace elements that varied between sites. This pattern was consistent across the study sites, especially in the very low cosine similarity in nitrate and ammonium, where DDM often returned negative sensitivities. Returning to this concept, we now examine how source compositions change between profile methods and how overall species importance changes between profile methods and sites.

Figure 9 compares these sources' variability between profile methods on a species basis with the coefficient of variation metric. As the coefficient of variation is the ratio of the sample standard deviation to the sample mean, the range of values for this metric begins at 0 and approaches infinity with small means. This metric should also be interpreted within the context of each source individually, as the sample means can change dramatically with source composition. Therefore, we define a value for each source group that indicates significantly increased variance

from the sample group equal to the group's 75th percentile value, as the distributions of the samples have a substantial right skew.

In AG, a source contributing solely to secondary species, the variation was lower across optimized profiles, though several sites did have values over the significance threshold of 1.37%: Boise with every secondary species except nitrate and Las Vegas and Reno with every secondary species. Of these sites, Las Vegas had the greatest mean variation, 14.8% of the mean. Windblown dust had relatively higher secondary species variation than all primary species, but this was approximately equal to the mean variation in Cu through Pb (all of which were derived from CMAQ unspeciated $PM_{2.5}$). Only two sites had mean variation greater than the DUS threshold of 29.3%, Fresno (33.9%) and Sacramento (31.2%).

The highest variation of the four sources presented here was in NG, which had a 75th percentile value of 40.3%. This variation was highest in primary species, though variations for nitrate and ammonium in Modesto surpassed the 75th percentile threshold. The mean variation of NG in Visalia also surpassed the mark at 48.3% of the mean. OTH had the second highest mean variation of the four sources, 23.8%, which is reasonable given that it contains the greatest number and diversity of sources in this study. There was an over 10 percentage point difference between mean primary (25.7%) and secondary (16.6%) species variations in this source despite some low primary variations in Cl, Br, and Pb due to large variations in species such as Sn and Ti in the California sites (Bakersfield, Fresno, Modesto and Sacramento).

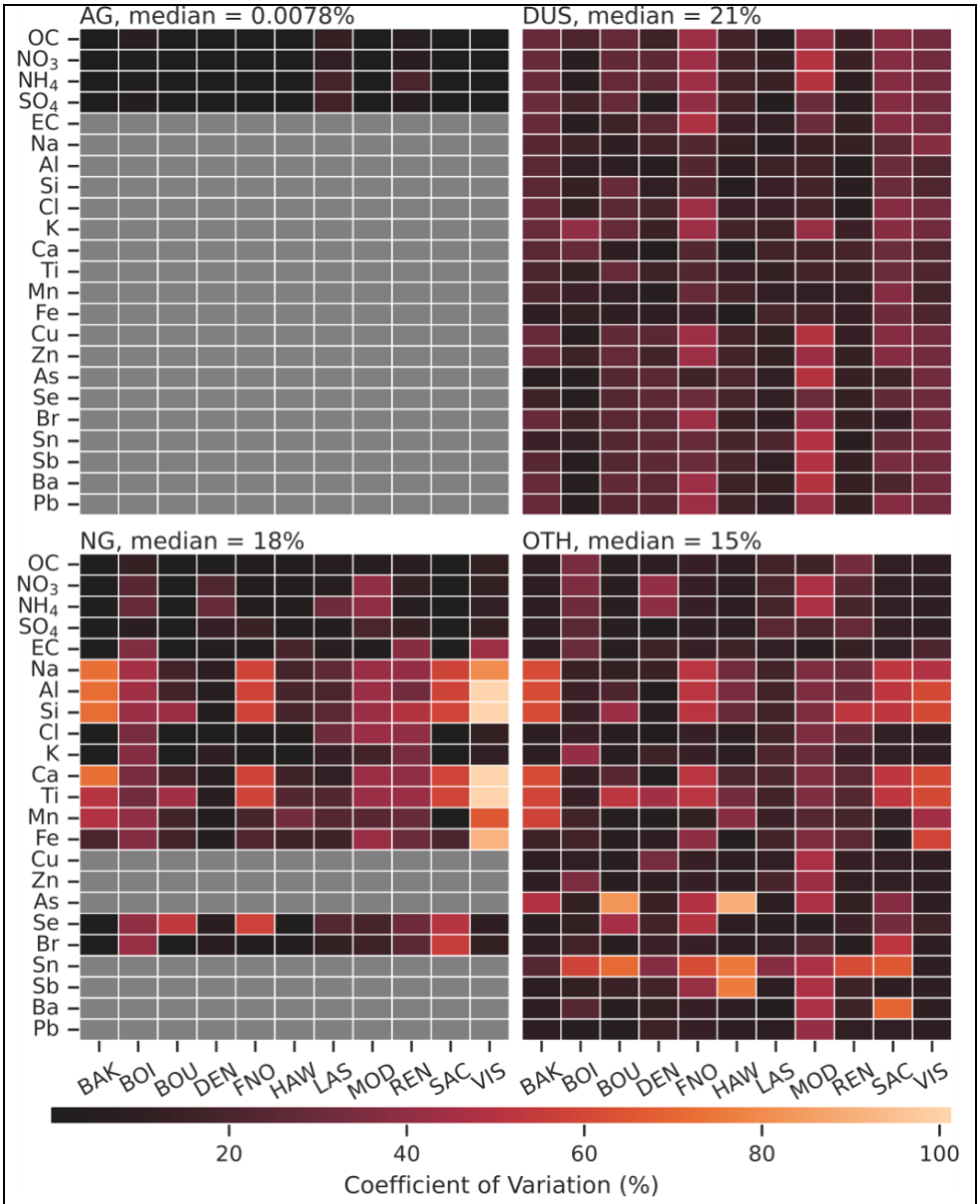

Figure 9 Coefficients of variation within optimized profiles and the standard seed profile at all study sites for agriculture (AG), windblown dust (DUS), natural gas (NG), and other sources (OTH). Gray squares indicate that the species in question is not a component of the source profile.

Returning to species with large variations in sensitivity, Figure 10 gives a summary of changes in species fingerprints between profiles at all sites. Here, a fingerprint is defined as the sum of impacts for a species across a site's profile (the sum of $f_{i,j}$ for all sources j and one species i), which can be taken as a rough metric for the relative importance of that chemical species in the site profile and should correspond with both the species' measured concentration and its sensitivities from CMAQ-DDM or CMAQ-ISAM (i.e., c_i^{obs} and $SA_{i,j}^{base}$ from Eq. 1).

The major components of $PM_{2.5}$ at all sites were OC, nitrate, EC, ammonium, and sulfate, with OC and nitrate being the largest of these species at all sites. Accordingly, OC fingerprints increased from the standard seed the most on average in all profiles: raw DDM with 0.181 g/g, non-negative DDM with 0.687 g/g and ISAM with 0.597 g/g. Conversely, while nitrate was the largest $PM_{2.5}$ component at Bakersfield, Boise, Bountiful, Denver, Hawthorne, and Visalia, its average increase from the standard seed at those sites was much smaller than OC, though on average it did increase from the standard seed. We see similar behavior for ammonium with smaller magnitudes. The other major components of $PM_{2.5}$, EC, and sulfate, also saw increases in fingerprints, but had large decreases at certain sites for certain profiles, such as sulfate in Modesto or EC in Visalia using the constrained DDM profile. Between the three optimized profiles, the raw DDM fingerprints changed the least from the standard seed, while the constrained DDM had large changes in both negative and positive directions from the standard seed.

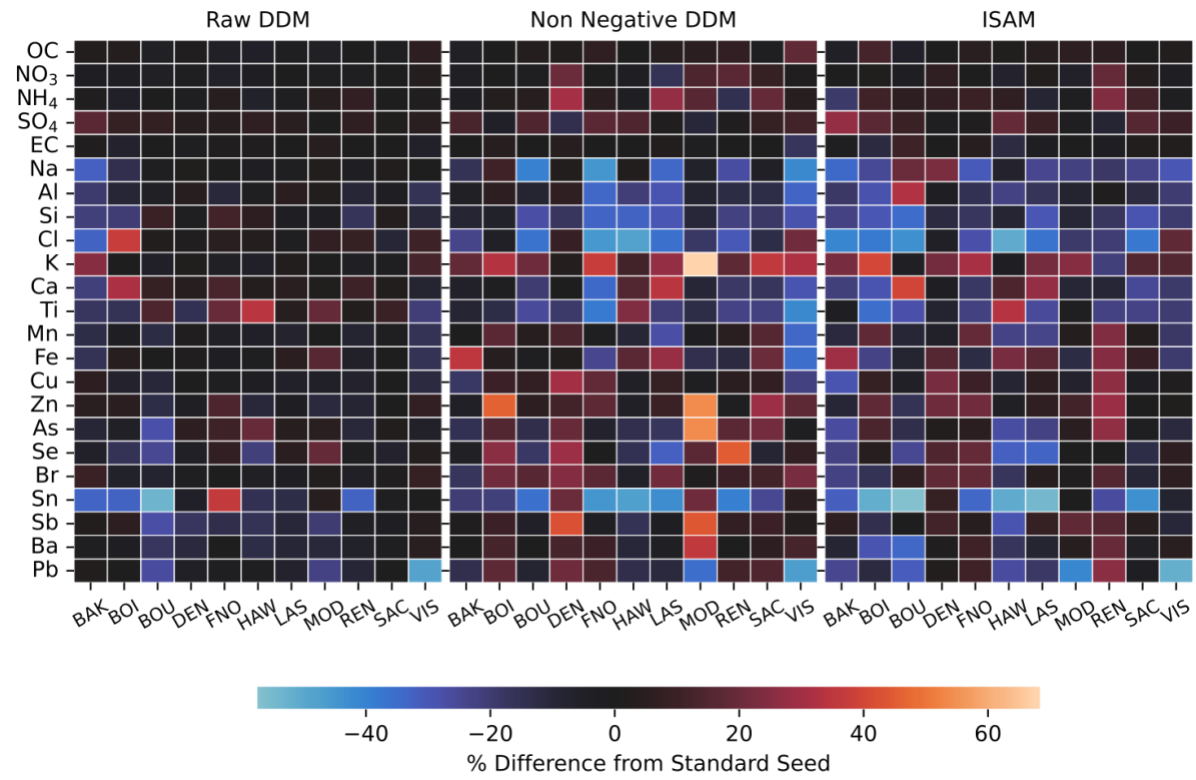

Figure 10 Relative differences in species fingerprints between the raw DDM (left), non-negative DDM (middle), and ISAM (right) profiles and the standard seed profile, in terms of the seed profile.

3.4 ISAM-Derived Source Profiles over January 2016

As ISAM apportionment data were available for the whole month of January 2016, we examined how optimized profiles change for a site during inversion episodes, which coincided with CSN observations at every site. PCAP and non-PCAP profiles were generated by individually optimizing profiles with CMAQ-ISAM data and CSN observations for every day in the month, then computing the mean of profiles for PCAPs and non-PCAPs using the PCAP/non-PCAP flags presented in Table S-4. Each average profile was created using at least two 24-hour profiles.

In Figure 11, the change in species fingerprints from the standard seed is presented for the averaged PCAP and non-PCAP profiles at the ten sites with both profiles. The largest absolute changes are found in already-abundant species, such as OC and sulfate, but the impact of concentration magnitude is dampened in Figure 11 as the data are normalized by standard seed species fingerprints. In general, secondary species fingerprints increased from the seed regardless of inversion conditions, with some exceptions for sulfate.

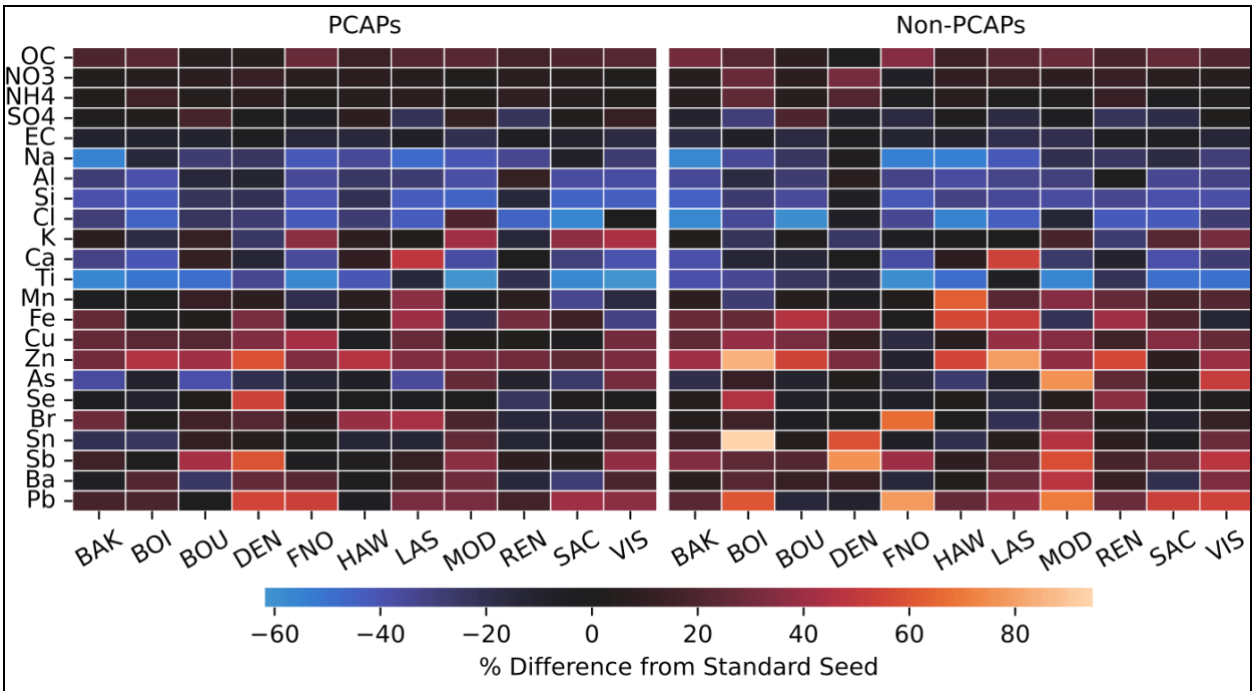

Figure 11 Percent differences between PCAP (left) and non-PCAP (right) average profiles versus the standard seed profile, in terms of the seed profile.

In trace species, there was no real pattern in which species increased or decreased versus the seed, and those species changed in the same direction regardless of inversions. Of the twenty-three $PM_{2.5}$ species, only four had increased fingerprints during PCAPs: sulfate (mean difference of 7.95% of standard seed during PCAPs vs non-PCAPs), EC (mean difference of 1.31%), Cl (mean difference of 4.75%), and K (mean increase of 8.89%). The species with the largest decreases in fingerprints during PCAPs were Sn (23.68% decrease), As (19.08% decrease), and

Mn (14.27% decrease). The largest individual changes in any direction were Sn (118.8% decrease at Boise), Pb (64.33% increase at Denver), and Br (63.69% increase at Las Vegas). The overall mean difference between PCAP and non-PCAP profiles was -4.97% of standard seed fingerprints.

Interestingly, the two halogen species (Cl and Br) had the largest increases in fingerprints during PCAPs; 75th percentile values of the profile differences were each approximately 25% of the standard seed fingerprint. Increases in Cl fingerprints were found in optimized January 1 profiles at Boise, Denver, and Visalia. Boise and Denver had decreased Cl fingerprints from the standard seed during PCAPs (-44.6% and -26.9%, respectively) during PCAPs, and the only site with increased PCAP Cl fingerprints was Modesto (+19.9%). These fingerprints increased during non-PCAP periods but still decreased from the standard seed by 34.5% and 6.0%. Cl fingerprints were 13.0% higher on average in PCAP profiles relative to non-PCAP profiles, with Bountiful (+86.2%) and Hawthorne (+62.6%) having the largest increases compared to the largest decreases at Fresno (-30.9%) and Sacramento (-29.7%). Br fingerprints increased from the standard seed in January 1 profiles at Boise, Bountiful, Denver, Fresno, Las Vegas, Sacramento, and Visalia.

The averaged PCAP fingerprints for Br increased at every site except Reno (-14.2%) and Sacramento (-7.8%) with a sitewide mean increase from the seed of 15.1%. During non-PCAP episodes, the Br fingerprint increased from the standard seed at Bakersfield (5.4%), Boise (14.3%), Fresno (32.7%), Modesto (27.6%), and Reno (4.3%). Br fingerprints were 13.8% higher on average for PCAP profiles relative to non-PCAP profiles, with the largest increases at Las Vegas (+80.4%) and Hawthorne (+38.9%) and the largest decreases at Fresno (-23.7%) and Reno (-17.8%). The large increases in halogen importance for Bountiful and Hawthorne in PCAP profiles meshes well with work observing regional halogen emission fluxes that lead to significant increases in regional oxidant and $PM_{2.5}$ concentrations during the wintertime.[20,21] Also of note is that the two major sources discussed in these studies come from playa dust (DUS) and an industrial magnesium refinery (MET).[20,21]

Figure 12, below, compares the cosine similarity of PCAP and non-PCAP composite profiles to the standard seed profile. Interestingly, the range of similarity values in this dataset does not change from the comparison of January 1 profiles in Figure 3.08, but the specific sources that have low similarities did change with the new profiles. The similarities in OTH continued to be notably low for PCAPs and non-PCAPs, and DUS, MET, and SOL were consistently low for both profiles and most sites. Furthermore, natural gas (NG), which was one of the most diverging sources in the January 1 profiles, did not dip below the similarity threshold of 0.95 in either of the averaged profiles, though NG was not a particularly dissimilar source profile in the ISAM comparisons with the standard seed. The similarity between PCAP-averaged ISAM and the standard seed ODE source profiles also increased from the single-day profile, where BOU similarities were greater than the 0.95 threshold during and in absence of PCAPs. This may be a result of the small sample size, as there were four PCAP profiles and two non-PCAP profiles for the whole study period. When comparing individual profiles to the standard seed, we find that ODE similarity values were as low as 0.93 during a PCAP on January 31 and 0.91 on January 25,

which was not a PCAP day. This increased agreement with the standard seed in aggregate is likely not a result of regression to the mean, but rather an impact of small sample sizes and perhaps the "weak" rather than "strong" PCAP flag for Bountiful/Hawthorne on January 1. More simulation time or speciated $PM_{2.5}$ data points would be necessary to fully understand this behavior.

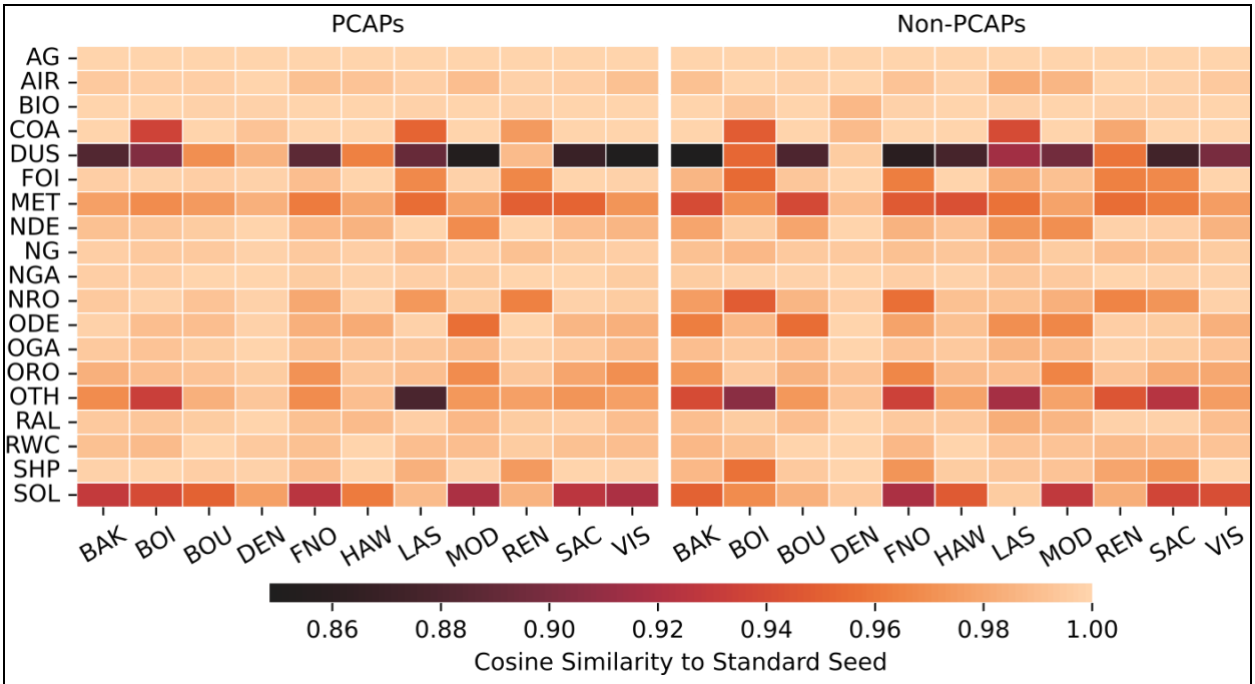

Figure 12 Cosine similarity of PCAP (left) and non-PCAP (right) profiles to the standard seed profile. We defined a threshold for similar profiles of cosine similarity values greater than or equal to 0.95.

The sources that we would expect to contribute chiefly to secondary $PM_{2.5}$, such as AG and (to a lesser extent in wintertime) BIO, have high similarity to the standard seed across the board. Another contributor to secondary $PM_{2.5}$, coal combustion (COA) was very dissimilar to the seed in many of the January 1 ISAM profiles but was mostly above the threshold for similarity in the composite profiles presented here. The sources with the lowest similarity values, DUS and SOL, both had seed source compositions with a mix of trace species (Se and Pb) and secondary species (see Figure 2), the perturbations of which could create a large change in the cosine similarity of the source profiles. Figure 10 did show that the largest relative changes in species fingerprints were in the less-abundant species towards the bottom of the profile matrix, including several of the more variable trace species discussed in Section 3.3, such as Sn, Ti, Se, and Pb.

The species with the greatest absolute differences between PCAP and non-PCAP profiles was sulfate, which increased in contributions to BIO, COA, FOI, NG, OTH, and SHP during PCAPs. OC increased contributions in DUS, ORO, and SOL and EC increased in NDE and ODE as well. Changes in an individual species' contribution to a source were less than 0.04 g/g in either direction. Relative differences between PCAP and non-PCAP profiles were less than 25% in either direction, with species that increased in importance during PCAPs including sulfate, chlorine, and

bromine. The increase in halogen contributions to sources during PCAPs may be attributable to the titration of oxidants over the course of a PCAP, leading to increased heterogeneous reactions of halogen species with nitrate and organic aerosol[21,41]

3.5 Sensitivity to Mobile Source Changes in Optimization Seeds

While the standard seed profile used in the DDM and initial ISAM optimizations is a common starting point for profile development,[17] California's notably stringent regulations on fuel composition and vehicle emission control devices could be significant when considering aged profile development that incorporates source impacts on secondary $PM_{2.5}$. In Figure 13, we compare the coefficient of variation between optimized on-road combustion (diesel and gasoline) profiles at all five California sites on January 1, 2016. The threshold values, or 75th percentiles, for these sources were 126% (ODE) and 58.7% (OGA).

The highest variance species at all sites, nitrate for OGA and ammonium for ODE, are both secondary species. Both species had variances over their group thresholds at all sites; ODE ammonium was 27.6 to 34.5 percentage points over its source threshold and OGA nitrate was 39.3 to 46.6 percentage points over the OGA threshold. This is promising for future apportionment in the CMB model during California inversion episodes, as ammonium nitrate is a major component of $PM_{2.5}$ in the Central Valley and other areas of California.[42–44] Interestingly, the coefficient of variation was much higher for on-road diesel profiles, with the lowest being 12% and each site had at least eight species with coefficient of variance over 100%. On the other hand, on-road gasoline profiles had relatively uniform coefficients of variance across most species on the order of 50%.

Other species that surpassed the ODE threshold of 126% variation were nitrate (at four of the five sites) as well as Na, Al, K, and Se (at all five sites). For OGA Na, Cl, and Ba were over the threshold at one site; Ca, Mn, and Fe at two sites; Al, Si, and Sn at three sites; and Ti at four sites. VIS had the fewest species (7) meet the variation threshold at either of the sources, followed by BAK (9), and the remaining sites had 14 out of 46 species over one of the source variation thresholds.

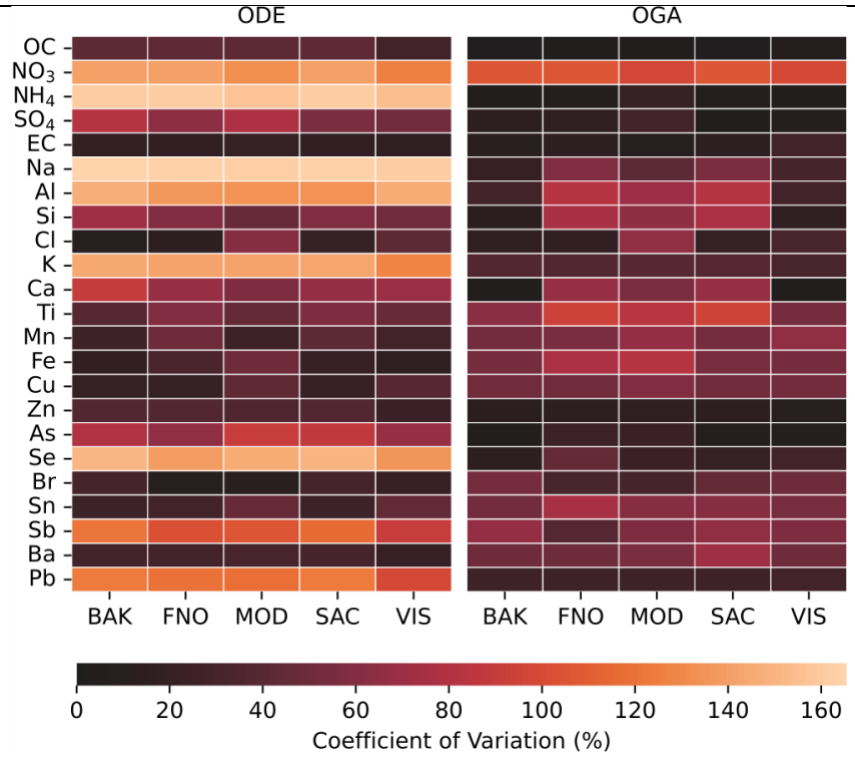

Figure 13 Coefficient of variation between optimized on-road gasoline (left) and on-road diesel (right) profiles at all California sites.

Figure 14, below, compares the cosine similarity of re-optimized ISAM profiles (CA ISAM) profiles to the standard seed profile at the five California sites. Across all sites we see that optimized DUS profiles have very low similarity to either the standard seed or the CA seed, echoing results for standard seed optimized profiles in section 3.3.3, above. We also see that optimized NDE and ODE profiles have much lower similarity to the standard seed than to the CA seed, proving that the changes to these initial points in optimization process can lead to markedly different results in the final profiles. However, this behavior is not seen for the gasoline profiles NGA and OGA, which were modified in the same way for the CA seed but only have a 0.3 to 1% change in similarity for OGA and essentially no change in NGA.

When comparing the results in Figure 14 with the similarity between the two seed profiles, we find that the similarity values for NGA (0.996) and OGA (0.991) are much higher than their diesel equivalents NDE (0.887) and ODE (0.876) and certainly meet the similarity threshold of 0.95. From this, we can see that the difference between the diesel and gas profile results does make sense. Finally, we also observe that the trends in similarity are not quite uniform across the five sites, where MOD often has lower similarity to each seed profile than the rest of the group, and its relative change in similarity across seed profiles for the modified mobile sources is also distinct. Modesto was one of the three sites tied for first place in species variation, which could contribute

to this behavior here. The other two sites with high species variation, Fresno and Sacramento, also show some differences in cosine similarity for certain sources (MET, NRO, ORO, and SHP).

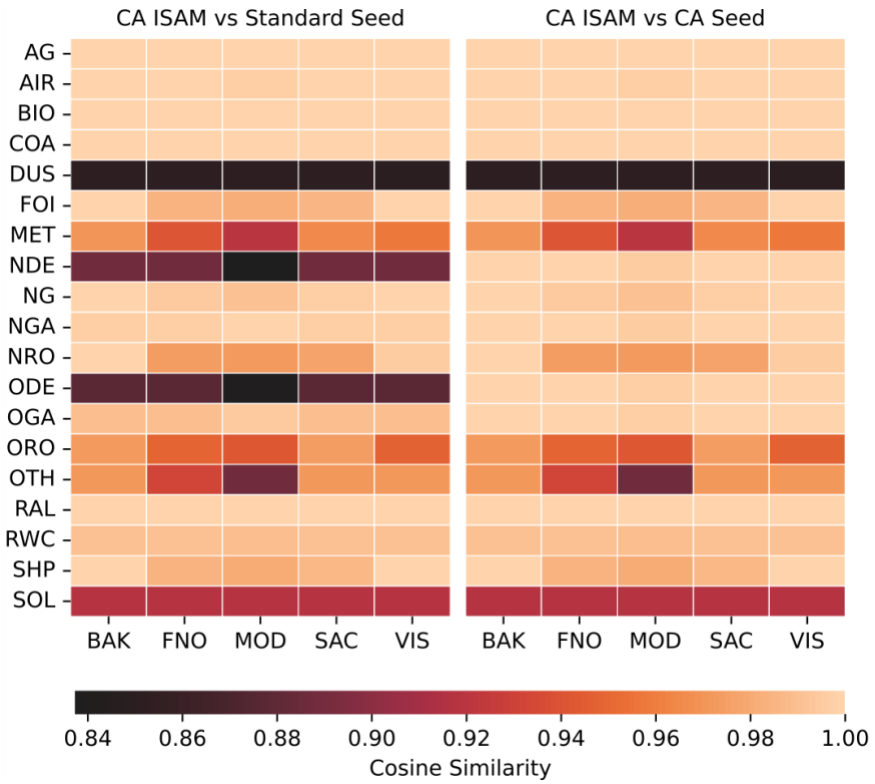

Figure 14 Cosine similarities of CA ISAM profiles to the standard seed and CA seed profiles (see Figs. 2 and 3, respectively) for each of the 19 sources. The only sources that were modified to create the CA seed are NDE, NGA, ODE, and OGA.

3.6. Summary, Limitations, and Future Work

The sources most sensitive to profile method choices were, surprisingly, not sources that consisted of largely secondary $PM_{2.5}$ species. Instead, sources like DUS, MET, and OTH had the largest variation among optimized profiles along with COA, which is associated with higher-abundance species like sulfate, OC, and nitrate. These results suggest that optimization inputs, such as measured concentrations and CMAQ sensitivities, can result in more inter-method variation for sources containing less-abundant primary species. Similarly, we found that the optimized profiles had the greatest mean impacts on OC, Si, and Ti on an absolute basis and Ti, Na, and K on a relative basis compared to the standard seed. As the bulk of modeled and observed $PM_{2.5}$ mass during the study period was secondary species and EC, one might expect that those species would experience the greatest changes with profile method. However, when these changes were normalized by the standard seed, we found that many trace species, such as Se, had over 100% changes in their fingerprints with some methods. These findings agree with other work observing variances of up to 400% in trace species, including dust Ca.[17] We saw the greatest

differences across PCAP and non-PCAP profiles for halogen species Cl and Br, especially in the Salt Lake Valley sites Bountiful and Hawthorne. These results emphasize the importance of the playa dust and industrial smelter emissions pathways to PCAP chemistry in this air basin.[20,21]

When experimenting with a different initial seed modified to match observations of California gasoline and diesel mobile source emissions, we found that the optimization process was sensitive to these changes. However, the sensitivity of profiles to these changes varied with fuel type; on and off-road diesel profiles from CA ISAM had the lowest similarities to the standard seed but had better agreement with the modified CA seed. CA ISAM profiles also showed the same divergence from both seed profiles in DUS and MET sources, echoing the behavior of profiles developed with the standard seed. This result calls for a more tailored, location-based approach to seed selection when developing optimized profiles as opposed to using a standard. This may be more difficult to implement in areas without distinct regulations, but even alterations to a few seed source profiles based on observational data can have an impact on the final, optimized product.

The methodology and results presented here do have some limitations which could be addressed in future work. CMAQ, one of the site-specific inputs to the optimization process, has well-documented issues in its simulations of wintertime pollution in mountain valleys and during inversions. These issues are often exacerbated by the coarse resolution of model grids, which also limits the number of observation sites that can be reasonably used in simultaneous analyses. The introduction of CMAQ-ISAM in 2013 and its continued use since release also raises questions as to the viability of CMAQ-DDM in this application.[45] For example, ISAM is not prone to the same numerical instability as DDM, and it was specifically designed for source apportionment applications. Since both models have comparable computational expenses, storage requirements, and input data, there is a preference for using ISAM alone in future work.

Turning to speciated $PM_{2.5}$ observations, another key input to the optimization process, one obvious limiting factor is the low time resolution of CSN data. The one-in-three-day or one-in-six-day sampling frequency does not always align with conditions that are beneficial to study. Such was the case with VIS in this work where no observation days coincided with inversion episodes, making the development of a PCAP profile at that site impossible without expensive, additional simulations. We also find that many of the source sectors examined in this study are collinear and emit chemical species in similar proportions, making simultaneous apportionment in CMB or similar programs difficult. Finally, the filter-based method used by CSN and IMPROVE has been shown to systemically underestimate ammonium and nitrate concentrations, especially in California.[42–44] As ammonium nitrate is a large component of wintertime $PM_{2.5}$ in the western U.S., this deficit in mass could cascade through the optimization process (leading to an underestimation of source impacts on secondary pollution) and into the source apportionment process (leading to misattribution of important, abundant pollutants).

The workflow and methods for this application in future work could be improved in several ways. Firstly, CMAQ-ISAM's stability would support longer and/or higher resolution simulations.

These improvements would allow for the independent optimization of dense observation sites or, in the case of longer simulation periods, partially address the issue of observations not capturing key events like PCAP episodes. Some improvements that could be made to the observations used in this application include the use of continuous monitors, such as an aerosol mass spectrometer (AMS), which would address the issue of observations missing key atmospheric conditions and allow for novel analysis of source impacts over diurnal cycles.

Acknowledgements

Research reported in this manuscript was in part supported by the National Institute of Environmental Health Sciences of the National Institutes of Health under award number R01ES032810. This research used the Savio computational cluster resource provided by the Berkeley Research Computing program at the University of California, Berkeley (supported by the UC Berkeley Chancellor, Vice Chancellor for Research, and Chief Information Officer).

References

(1) US EPA, O. *National Ambient Air Quality Standards (NAAQS) for PM*. https://www.epa.gov/pm-pollution/national-ambient-air-quality-standards-naaqs-pm (accessed 2024-04-29).

(2) Wang, Y.; Marshall, J. D.; Apte, J. S. U.S. Ambient Air Monitoring Network Has Inadequate Coverage under New PM2.5 Standard. *Environ. Sci. Technol. Lett.* **2024**, *11* (11), 1220–1226. https://doi.org/10.1021/acs.estlett.4c00605.

(3) Wang, Y.; Apte, J. S.; Hill, J. D.; Ivey, C. E.; Patterson, R. F.; Robinson, A. L.; Tessum, C. W.; Marshall, J. D. Location-Specific Strategies for Eliminating US National Racial-Ethnic PM2.5 Exposure Inequality. *Proc. Natl. Acad. Sci.* **2022**, *119* (44), e2205548119. https://doi.org/10.1073/pnas.2205548119.

(4) Shi, G.; Liu, J.; Wang, H.; Tian, Y.; Wen, J.; Shi, X.; Feng, Y.; Ivey, C. E.; Russell, A. G. Source Apportionment for Fine Particulate Matter in a Chinese City Using an Improved Gas-Constrained Method and Comparison with Multiple Receptor Models. *Environ. Pollut.* **2018**, *233*, 1058–1067. https://doi.org/10.1016/j.envpol.2017.10.007.

(5) Hakami, A.; Zhao, S.; Soltanzadeh, M.; Vasilakos, P.; Alhusban, A.; Oztaner, B.; Fann, N.; Chang, H.; Krupnick, A.; Russell, T. Estimating Model-Based Marginal Societal Health Benefits of Air Pollution Emission Reductions in the United States and Canada. *Res. Rep. Health Eff. Inst.* **2024**, *2024*, 218.

(6) Ivey, C.; Holmes, H.; Shi, G.; Balachandran, S.; Hu, Y.; Russell, A. G. Development of PM2.5 Source Profiles Using a Hybrid Chemical Transport-Receptor Modeling Approach. *Environ. Sci. Technol.* **2017**. https://doi.org/10.1021/acs.est.7b03781.

(7) Ivey, C. E.; Balachandran, S.; Colgan, S.; Hu, Y.; Holmes, H. A. Investigating Fine Particulate Matter Sources in Salt Lake City during Persistent Cold Air Pool Events. *Atmos. Environ.* **2019**, *213*, 568–578. https://doi.org/10.1016/j.atmosenv.2019.06.042.

(8) Balachandran, S.; Pachon, J. E.; Hu, Y.; Lee, D.; Mulholland, J. A.; Russell, A. G. Ensemble-Trained Source Apportionment of Fine Particulate Matter and Method Uncertainty Analysis. *Atmos. Environ.* **2012**, *61*, 387–394. https://doi.org/10.1016/j.atmosenv.2012.07.031.

(9) Whiteman, C. D.; Hoch, S. W.; Horel, J. D.; Charland, A. Relationship between Particulate Air Pollution and Meteorological Variables in Utah's Salt Lake Valley. *Atmos. Environ.* **2014**, *94*, 742–753. https://doi.org/10.1016/j.atmosenv.2014.06.012.

(10) Holmes, H. A.; Sriramasamudram, J. K.; Pardyjak, E. R.; Whiteman, C. D. Turbulent Fluxes and Pollutant Mixing during Wintertime Air Pollution Episodes in Complex Terrain. *Environ. Sci. Technol.* **2015**, *49* (22), 13206–13214. https://doi.org/10.1021/acs.est.5b02616.

(11) Colgan, S.; Sun, X.; Holmes, H. A. A Novel Meteorological Method to Classify Wintertime Cold-Air Pool Events. *Atmos. Environ.* **2021**, *261*, 118594. https://doi.org/10.1016/j.atmosenv.2021.118594.

(12) Boomsma, J.; Holmes, H. A. Leveraging Meteorological Reanalysis Models to Characterize Wintertime Cold Air Pool Events Across the Western United States from 2000 to 2022. *Atmosphere* **2025**, *16* (12), 1325. https://doi.org/10.3390/atmos16121325.

(13) Baasandorj, M.; Hoch, S. W.; Bares, R.; Lin, J. C.; Brown, S. S.; Millet, D. B.; Martin, R.; Kelly, K.; Zarzana, K. J.; Whiteman, C. D.; Dube, W. P.; Tonnesen, G.; Jaramillo, I. C.; Sohl, J. Coupling between Chemical and Meteorological Processes under Persistent Cold-Air Pool Conditions: Evolution of Wintertime $PM_{2.5}$ Pollution Events and N_2O_5

Observations in Utah's Salt Lake Valley. *Environ. Sci. Technol.* **2017**, *51* (11), 5941–5950. https://doi.org/10.1021/acs.est.6b06603.
(14) Ivey, C. E.; Holmes, H. A.; Hu, Y.; Mulholland, J. A.; Russell, A. G. A Method for Quantifying Bias in Modeled Concentrations and Source Impacts for Secondary Particulate Matter. *Front. Environ. Sci. Eng.* **2016**, *10* (5). https://doi.org/10.1007/s11783-016-0866-6.
(15) Henneman, L. R. F.; Choirat, C.; Ivey, C.; Cummiskey, K.; Zigler, C. M. Characterizing Population Exposure to Coal Emissions Sources in the United States Using the HyADS Model. *Atmos. Environ.* **2019**, *203*, 271–280. https://doi.org/10.1016/j.atmosenv.2019.01.043.
(16) Huang, M.; Ivey, C.; Hu, Y.; Holmes, H. A.; Strickland, M. J. Source Apportionment of Primary and Secondary PM2.5: Associations with Pediatric Respiratory Disease Emergency Department Visits in the U.S. State of Georgia. *Environ. Int.* **2019**, *133*, 105167. https://doi.org/10.1016/j.envint.2019.105167.
(17) Ivey, C.; Holmes, H.; Shi, G.; Balachandran, S.; Hu, Y.; Russell, A. G. Development of PM2.5 Source Profiles Using a Hybrid Chemical Transport-Receptor Modeling Approach. *Environ. Sci. Technol.* **2017**, *51* (23). https://doi.org/10.1021/acs.est.7b03781.
(18) Kaur, K.; Krall, J. R.; Ivey, C.; Holmes, H. A.; Kelly, K. E. Impact of Chemical Speciation Network Method Changes on Time Series Ion and Carbon Species Concentrations. *Aerosol Sci. Technol.* **2024**, *58* (11), 1318–1332. https://doi.org/10.1080/02786826.2024.2384921.
(19) Kaur, K. Long Term (2000-2020) Source Apportionment at 12 Western United States DRAFT. **2025**.
(20) Christie, J. A.; Elliott, H. E.; O'Connell-Lopez, S. M. O.; Perry, K.; Pratt, K. A.; Hallar, A. G.; Hrdina, A.; Murphy, J. G.; Riedel, T. P.; Long, R. W.; Mitroo, D.; Haskins, J. D.; Gaston, C. J. Halogen Production from Playa Dust Emitted from the Great Salt Lake: Implications of the Shrinking Great Salt Lake on Regional Air Quality. *ACS Earth Space Chem.* **2025**, *9* (3), 480–493. https://doi.org/10.1021/acsearthspacechem.4c00258.
(21) Womack, C. C.; Chace, W. S.; Wang, S.; Baasandorj, M.; Fibiger, D. L.; Franchin, A.; Goldberger, L.; Harkins, C.; Jo, D. S.; Lee, B. H.; Lin, J. C.; McDonald, B. C.; McDuffie, E. E.; Middlebrook, A. M.; Moravek, A.; Murphy, J. G.; Neuman, J. A.; Thornton, J. A.; Veres, P. R.; Brown, S. S. Midlatitude Ozone Depletion and Air Quality Impacts from Industrial Halogen Emissions in the Great Salt Lake Basin. *Environ. Sci. Technol.* **2023**, *57* (5), 1870–1881. https://doi.org/10.1021/acs.est.2c05376.
(22) Phelan, C. M.; Lawal, A. S.; Boomsma, J.; Kaur, K.; Kelly, K. E.; Holmes, H. A.; Ivey, C. E. Analyzing the Role of Chemical Mechanism Choice in Wintertime $PM_{2.5}$ Modeling for Temperature Inversion-Prone Areas. *ACS EST Air* **2025**, acsestair.4c00139. https://doi.org/10.1021/acsestair.4c00139.
(23) Byun, D.; Schere, K. L. Review of the Governing Equations, Computational Algorithms, and Other Components of the Models-3 Community Multiscale Air Quality (CMAQ) Modeling System. *Appl. Mech. Rev.* **2006**, *59* (2), 51. https://doi.org/10.1115/1.2128636.
(24) Napelenok, S. L.; Cohan, D.; Hu, Y.; Russell, A. G. Decoupled Direct 3D Sensitivity Analysis for Particulate Matter (DDM-3D/PM). *Atmos. Environ.* **2006**, *40* (32), 6112–6121. https://doi.org/10.1016/j.atmosenv.2006.05.039.
(25) Reff, A.; Bhave, P. V.; Simon, H.; Pace, T. G.; Pouliot, G. A.; Mobley, J. D.; Houyoux, M. Emissions Inventory of PM 2.5 Trace Elements across the United States. *Environ. Sci. Technol.* **2009**, *43* (15), 5790–5796. https://doi.org/10.1021/es802930x.

(26) *CMAS: Community Modeling and Analysis System*. https://www.cmascenter.org/smoke/ (accessed 2025-07-31).
(27) *Utah Office of Administrative Rules*. https://adminrules.utah.gov/public/rule/R307-202/Current%20Rules?# (accessed 2025-07-30).
(28) Stephens, Ryan. *Utah Division of Air Quality 2016 Annual Report*; Annual Report DAQ-2017-001541; Utah Division of Air Quality (DAQ), 2017. https://lf-public.deq.utah.gov/WebLink/DocView.aspx?id=392089&repo=Public (accessed 2024-09-12).
(29) Kelly, K. E.; Kotchenruther, R.; Kuprov, R.; Silcox, G. D. Receptor Model Source Attributions for Utah's Salt Lake City Airshed and the Impacts of Wintertime Secondary Ammonium Nitrate and Ammonium Chloride Aerosol. *J. Air Waste Manag. Assoc.* **2013**, *63* (5), 575–590. https://doi.org/10.1080/10962247.2013.774819.
(30) Kelly, K. E.; Kotchenruther, R.; Kuprov, R.; Silcox, G. D. Receptor Model Source Attributions for Utah's Salt Lake City Airshed and the Impacts of Wintertime Secondary Ammonium Nitrate and Ammonium Chloride Aerosol. *J. Air Waste Manag. Assoc.* **2013**, *63* (5), 575–590. https://doi.org/10.1080/10962247.2013.774819.
(31) Jaramillo, I. C.; Daher, N.; Kelly, K. Understanding How Wood-Burning's Contributions to Particulate Matter Concentrations Have Changed over Time.
(32) Baasandorj, M.; Brown, S.; Hoch, S.; Crosman, E.; Long, R.; Silva, P.; Mitchell, L.; Hammond, I.; Martin, R.; Bares, R.; Lin, J.; Sohl, J.; Page, J. 2017 Utah Winter Fine Particulate Study Final Report.
(33) Xu, L.; Suresh, S.; Guo, H.; Weber, R. J.; Ng, N. L. Aerosol Characterization over the Southeastern United States Using High-Resolution Aerosol Mass Spectrometry: Spatial and Seasonal Variation of Aerosol Composition and Sources with a Focus on Organic Nitrates. *Atmospheric Chem. Phys.* **2015**, *15* (13), 7307–7336. https://doi.org/10.5194/acp-15-7307-2015.
(34) *The California Reformulated Gasoline Regulations*; 2014; Vol. Title 13. https://ww2.arb.ca.gov/sites/default/files/2020-05/California_Reformulated_Gasoline_Regulations_2-16-14.pdf.
(35) California Air Resources Board Unofficial Diesel Fuel Regulations. *Title 13 Calif. Code Regul. Sect. 2281-2285 2299-22995 Title 17 Calif. Code Regul. Sect. 93114 93117 93118 931182 931183 931185* **2014**.
(36) Preble, C. V.; Harley, R. A.; Kirchstetter, T. W. Control Technology-Driven Changes to In-Use Heavy-Duty Diesel Truck Emissions of Nitrogenous Species and Related Environmental Impacts. *Environ. Sci. Technol.* **2019**, *53* (24), 14568–14576. https://doi.org/10.1021/acs.est.9b04763.
(37) Preble, C.; Harley, R.; Kirchstetter, T. Characterization of In-Use Heavy-Duty Diesel Truck Emission Rates Over the Past Decade—Emission Control Technology Performance; 2023; Vol. 2023, pp A23A-04.
(38) *Raising standards to lower diesel emissions | Science*. https://www.science.org/doi/10.1126/science.abf8159 (accessed 2025-08-04).
(39) Ansari, A. S.; Pandis, S. N. Response of Inorganic PM to Precursor Concentrations. *Environ. Sci. Technol.* **1998**, *32* (18), 2706–2714. https://doi.org/10.1021/es971130j.
(40) Phelan, C.; Lawal, A.; Ivey, C. CMAQ-DDM and CMAQ-ISAM Sensitivity Data Used for Profile Optimization, 2025. https://doi.org/10.5281/ZENODO.16914295.

(41) Simpson, W. R.; Brown, S. S.; Saiz-Lopez, A.; Thornton, J. A.; von Glasow, R. Tropospheric Halogen Chemistry: Sources, Cycling, and Impacts. *Chem. Rev.* **2015**, *115* (10), 4035–4062. https://doi.org/10.1021/cr5006638.
(42) Burns, A. M.; Chandler, G.; Dunham, K. J.; Carlton, A. G. Data Gap: Air Quality Networks Miss Air Pollution from Concentrated Animal Feeding Operations. *Environ. Sci. Technol.* **2023**, *57* (49), 20718–20725. https://doi.org/10.1021/acs.est.3c06947.
(43) Chiu, Y. T. T.; Carlton, A. G. Aerosol Thermodynamics: Nitrate Loss from Regulatory PM2.5 Filters in California. *ACS EST Air* **2024**, *1* (1), 25–32. https://doi.org/10.1021/acsestair.3c00013.
(44) Ward, R. X.; Baliaka, H. D.; Schulze, B. C.; Kerr, G. H.; Crounse, J. D.; Hasheminassab, S.; Bahreini, R.; Dillner, A. M.; Russell, A.; Ng, N. L.; Wennberg, P. O.; Flagan, R. C.; Seinfeld, J. H. Poorly Quantified Trends in Ammonium Nitrate Remain Critical to Understand Future Urban Aerosol Control Strategies. *Sci. Adv.* **2025**, *11* (21), eadt8957. https://doi.org/10.1126/sciadv.adt8957.
(45) Kwok, R. H. F.; Napelenok, S. L.; Baker, K. R. Implementation and Evaluation of PM2.5 Source Contribution Analysis in a Photochemical Model. *Atmos. Environ.* **2013**, *80*, 398–407. https://doi.org/10.1016/j.atmosenv.2013.08.017.

Supplemental Information for:

Novel Source Apportionment Methodologies for Secondary $PM_{2.5}$ during Extreme Wintertime Meteorological Conditions in the Western U.S.

Cam M. Phelan[1], Abiola S. Lawal[1†], Kamaljeet Kaur [2], Jenna Krall [3], Kerry E. Kelly [2], Heather A. Holmes [2] , and Cesunica E. Ivey[1]*

[1] Department of Civil and Environmental Engineering, University of California Berkeley, Berkeley, CA 94720 USA
[2] Department of Chemical Engineering, University of Utah, Salt Lake City, UT, 84112 USA
[3] Department of Global and Community Health, George Mason University, Fairfax, VA, 22030 USA
*Corresponding Author, iveyc@berkeley.edu
[†] Now at School of Civil and Environmental Engineering, University of Connecticut, Storrs, CT 06269 USA

Text S-1 Source profile optimization equations and constraints

The source profile optimization equation is derived from the chemical mass balance method[1]:

$$c_i^{obs} = \sum_{j=1}^{J} f_{i,j} S_j + e_i \,, \tag{S1}$$

$$c_i^{obs} = \sum_{j=1}^{J} r_{i,j} f_{i,j}^0 (\sum_{i=1}^{I} SA_{i,j}^{base}) + e_i \tag{S2}$$

where $f_{i,j}$ is the fraction of species *i* that is emitted from source *j*, S_j is the impact of source *j* on total $PM_{2.5}$, and e_i (*X* in Eq. S3) is the concentration prediction error to be minimized. Uncertainties and constraints are added to the objective function (Eq. S1) to weight and balance the prediction error:

$$X^2 = \sum_{i=1}^{I} \left(\frac{\left[c_i^{obs} - (\sum_{j=1}^{J} r_{ij} f_{ij}^0 SA_{i,j}^{base}) \right]^2}{{\sigma_{i,obs}}^2 + {\sigma_{i,SA}}^2} \right) + \alpha \Gamma \sum_{i=1}^{I} \left(\sum_{j=1}^{J} \left[\frac{f_{ij}^0 (r_{ij} - 1)}{\sigma_{f_{ij}}} * U(f_{ij}^0) \right]^2 \right) \tag{S3}$$

$${\sigma_{i,SA}}^2 = (\sum_{j=1}^{J} \sigma_{f_{i,j}^0} SA_{i,j}^{base} R_j)^2 \tag{S4}$$

$$U(f_{ij}^0) = \begin{matrix} 1, & |f_{ij}^0| > 0 \\ 0, & f_{ij}^0 = 0 \end{matrix} \tag{S5}$$

$$\sum_{i=1}^{I} r_{i,j} f_{i,j}^0 \leq 1 \tag{S6}$$

The variable ${\sigma_{i,SA}}^2$ is the uncertainty of the source impacts on species *i* (Eq. S4)*;* the variable $\sigma_{f_{i,j}^0}$ is the numerical uncertainty of the reference source profiles; α is a sensitivity term ($\alpha = \frac{I}{\sum_{i=1}^{I} \sum_{j=1}^{J} U(f_{ij}^0)}$ in this study); Γ is a numerical weighting term ($\Gamma = 0.01$ in this application); and $U(f_{ij}^0)$ is a piecewise function used to constrain the optimization and omit species with zero contribution from the source from having numerical influence on the optimization (Eq. S5). Adjustments yield profiles for which the sum of factional contributions is ≤ 1 for each source (Eq. S6).

Data Tables

Table S-1 Standard seed profile for optimization, split for formatting purposes. Data for sources other than AG and BIO are derived from observations in Reff et al., (2009). Blank cells are treated as zero in the nonlinear optimization workflow. All units are in g/g.

	AG*	AIR	BIO*	COA	DUS	FOI	MET	NDE	NG	NGA
OC	2.5E-02	1.8E-01	8.1E-01	3.9E-02	4.9E-02	1.1E-01	7.1E-02	1.8E-01	4.8E-01	4.8E-01
NO_3	6.7E-01	1.1E-03	9.0E-02	2.0E-03	1.8E-03	0.0E+00	5.2E-03	1.1E-03	3.3E-02	7.0E-04
NH_4	3.0E-01		0.0E+00	2.4E-02	8.6E-04	0.0E+00	4.1E-04		4.2E-03	0.0E+00
SO_4	3.2E-04	3.0E-03	9.9E-02	1.2E-01	6.0E-03	3.3E-01	1.8E-01	3.0E-03	1.2E-01	5.0E-04
EC	0.0E+00	7.7E-01	0.0E+00	2.1E-02	1.7E-03	4.9E-02	1.4E-02	7.7E-01	8.5E-02	1.2E-01
Na	0.0E+00		0.0E+00	1.2E-03	1.1E-03	0.0E+00	3.1E-02		2.0E-02	0.0E+00
Al	0.0E+00		0.0E+00	4.4E-02	5.9E-02	0.0E+00	3.5E-02		2.1E-03	0.0E+00
Si	0.0E+00		0.0E+00	8.0E-02	1.7E-01	3.5E-03	4.0E-02		2.6E-03	1.2E-03
Cl	0.0E+00	2.1E-04	0.0E+00	6.0E-03	1.4E-03	1.8E-03	1.0E-01	2.1E-04	3.7E-02	0.0E+00
K	0.0E+00	3.8E-05	0.0E+00	4.3E-03	1.7E-02	1.7E-04	3.7E-02	3.8E-05	1.6E-03	0.0E+00
Ca	0.0E+00	5.8E-04	0.0E+00	3.9E-02	5.4E-02	2.9E-04	1.3E-02	5.8E-04	9.8E-03	3.0E-04
Ti	0.0E+00	4.0E-06	0.0E+00	2.4E-03	3.9E-03	3.6E-04	8.9E-04	4.0E-06	9.4E-04	0.0E+00
Mn	0.0E+00		0.0E+00	1.8E-04	1.2E-03	2.1E-05	5.1E-03		1.9E-04	0.0E+00
Fe	0.0E+00	2.6E-04	0.0E+00	2.1E-02	4.4E-02	5.6E-04	7.5E-02	2.6E-04	8.5E-04	1.0E-04
Cu	0.0E+00		0.0E+00	1.5E-04	1.1E-04	8.7E-05	5.5E-03		0.0E+00	0.0E+00
Zn	0.0E+00	6.8E-04	0.0E+00	5.1E-04	5.2E-04	7.1E-04	2.6E-03	6.8E-04	0.0E+00	3.0E-04
As	0.0E+00	3.0E-06	0.0E+00	1.2E-06	1.8E-05	0.0E+00	4.1E-04	3.0E-06	0.0E+00	0.0E+00
Se	0.0E+00		0.0E+00	2.8E-03	1.1E-06	2.8E-05	1.7E-04		5.8E-04	0.0E+00
Br	0.0E+00	1.5E-05	0.0E+00	2.9E-04	1.2E-05	0.0E+00	1.4E-03	1.5E-05	3.8E-04	0.0E+00
Sn	0.0E+00	2.5E-05	0.0E+00	1.3E-04	2.8E-05	0.0E+00	3.8E-04	2.5E-05	0.0E+00	0.0E+00
Sb	0.0E+00	1.9E-05	0.0E+00	8.1E-06	3.2E-05	1.3E-04	8.2E-04	1.9E-05	0.0E+00	2.0E-04
Ba	0.0E+00	3.5E-04	0.0E+00	3.9E-03	7.9E-04	0.0E+00	2.8E-03	3.5E-04	0.0E+00	0.0E+00
Pb	0.0E+00	1.0E-06	0.0E+00	1.2E-04	2.2E-04	0.0E+00	2.1E-03	1.0E-06	0.0E+00	3.0E-04

	NRO	ODE	OGA	ORO	OTH	RAL	RWC	SHP	SOL
OC	2.1E-01	1.8E-01	4.1E-01	2.1E-01	1.1E-01	1.8E-01	4.2E-01	1.1E-01	2.7E-01
NO_3	1.3E-02	1.2E-03	1.5E-03	1.6E-03	9.2E-03	1.1E-03	7.8E-04	2.1E-08	3.6E-04
NH_4	1.7E-03	1.7E-04	1.0E-02	7.4E-05	7.2E-03	4.8E-09	6.1E-04	2.6E-09	7.5E-04
SO_4	2.9E-01	3.9E-03	1.8E-02	3.3E-02	1.4E-01	3.0E-03	4.0E-02	3.3E-01	2.8E-02
EC	9.3E-02	7.5E-01	1.5E-01	7.9E-02	2.6E-02	7.7E-01	4.5E-02	4.9E-02	4.7E-03
Na	8.1E-03	2.0E-05	7.6E-04	2.8E-04	3.8E-02	2.3E-08	1.3E-03	1.3E-08	2.4E-05
Al	8.3E-04	3.1E-05	1.3E-03	1.1E-03	1.3E-02	2.4E-09	4.5E-05	1.3E-09	2.5E-02
Si	1.1E-03	1.3E-03	2.9E-02	6.4E-02	3.8E-02	6.5E-08	8.0E-02	3.5E-03	2.5E-02
Cl	1.6E-02	3.4E-04	1.8E-03	3.2E-03	2.1E-02	2.1E-04	4.4E-03	1.8E-03	3.2E-03
K	6.5E-04	4.5E-05	2.1E-04	2.4E-04	1.7E-02	3.8E-05	5.6E-02	1.7E-04	2.0E-03
Ca	4.2E-03	7.1E-04	4.8E-03	7.6E-03	2.6E-02	5.8E-04	3.8E-03	2.9E-04	2.5E-02
Ti	7.3E-04	5.8E-05	1.1E-03	2.7E-03	4.3E-03	4.0E-06	0.0E+00	3.6E-04	1.7E-01
Mn	9.6E-05	1.6E-05	3.5E-04	8.1E-04	4.9E-04	2.2E-10	0.0E+00	2.1E-05	0.0E+00
Fe	5.2E-04	1.9E-03	3.7E-02	8.5E-02	8.0E-03	2.6E-04	3.7E-05	5.6E-04	3.3E-04
Cu	0.0E+00	1.7E-04	3.6E-03	8.5E-03	2.3E-04	0.0E+00	0.0E+00	8.7E-05	1.5E-05
Zn	9.5E-05	7.6E-04	2.7E-03	2.7E-03	6.8E-04	6.8E-04	9.0E-05	7.1E-04	1.1E-05
As	2.4E-07	3.1E-06	6.0E-06	7.3E-06	3.5E-05	3.0E-06	8.2E-07	0.0E+00	0.0E+00
Se	2.6E-04	5.8E-07	1.2E-05	2.0E-05	3.0E-05	6.7E-10	0.0E+00	2.8E-05	0.0E+00
Br	1.5E-04	1.5E-05	4.9E-05	3.3E-05	4.3E-04	1.5E-05	8.2E-06	2.4E-10	9.9E-05
Sn	2.0E-06	1.1E-04	2.0E-03	4.8E-03	7.9E-05	2.5E-05	4.1E-06	0.0E+00	0.0E+00
Sb	1.3E-04	2.0E-05	1.1E-04	0.0E+00	1.5E-04	1.9E-05	0.0E+00	1.3E-04	4.7E-03
Ba	2.8E-05	8.1E-04	1.1E-02	2.5E-02	6.2E-04	3.5E-04	0.0E+00	0.0E+00	1.3E-02
Pb	3.3E-07	7.6E-06	3.2E-04	8.0E-05	2.2E-04	1.0E-06	2.5E-06	0.0E+00	3.0E-04

Table S-2 Modified California seed profile. The only sources modified in this profile were NDE, NGA, ODE, and OGA. These modified columns are italicized and starred. All units are in g/g.

	AG	AIR	BIO	COA	DUS	FOI	MET	**NDE**	NG	**NGA**
OC	2.5E-02	1.8E-01	8.1E-01	3.9E-02	4.9E-02	1.1E-01	7.1E-02	4.2E-01	4.8E-01	7.7E-01
NO_3	6.7E-01	1.1E-03	9.0E-02	2.0E-03	1.8E-03	0.0E+00	5.2E-03	2.1E-02	3.3E-02	8.3E-03
NH_4	3.0E-01		0.0E+00	2.4E-02	8.6E-04	0.0E+00	4.1E-04		4.2E-03	0.0E+00
SO_4	3.2E-04	3.0E-03	9.9E-02	1.2E-01	6.0E-03	3.3E-01	1.8E-01	1.4E-02	1.2E-01	1.2E-03
EC	0.0E+00	7.7E-01	0.0E+00	2.1E-02	1.7E-03	4.9E-02	1.4E-02	4.9E-01	8.5E-02	2.7E-01
Na	0.0E+00		0.0E+00	1.2E-03	1.1E-03	0.0E+00	3.1E-02		2.0E-02	0.0E+00
Al	0.0E+00		0.0E+00	4.4E-02	5.9E-02	0.0E+00	3.5E-02		2.1E-03	0.0E+00
Si	0.0E+00		0.0E+00	8.0E-02	1.7E-01	3.5E-03	4.0E-02		2.6E-03	1.5E-03
Cl	0.0E+00	2.1E-04	0.0E+00	6.0E-03	1.4E-03	1.8E-03	1.0E-01	1.8E-04	3.7E-02	0.0E+00
K	0.0E+00	3.8E-05	0.0E+00	4.3E-03	1.7E-02	1.7E-04	3.7E-02	7.2E-04	1.6E-03	0.0E+00
Ca	0.0E+00	5.8E-04	0.0E+00	3.9E-02	5.4E-02	2.9E-04	1.3E-02	3.3E-03	9.8E-03	5.7E-04
Ti	0.0E+00	4.0E-06	0.0E+00	2.4E-03	3.9E-03	3.6E-04	8.9E-04	1.5E-05	9.4E-04	0.0E+00
Mn	0.0E+00		0.0E+00	1.8E-04	1.2E-03	2.1E-05	5.1E-03		1.9E-04	0.0E+00
Fe	0.0E+00	2.6E-04	0.0E+00	2.1E-02	4.4E-02	5.6E-04	7.5E-02	4.3E-04	8.5E-04	1.1E-05
Cu	0.0E+00		0.0E+00	1.5E-04	1.1E-04	8.7E-05	5.5E-03		0.0E+00	0.0E+00
Zn	0.0E+00	6.8E-04	0.0E+00	5.1E-04	5.2E-04	7.1E-04	2.6E-03	1.5E-03	0.0E+00	6.8E-04
As	0.0E+00	3.0E-06	0.0E+00	1.2E-06	1.8E-05	0.0E+00	4.1E-04	1.7E-05	0.0E+00	0.0E+00
Se	0.0E+00		0.0E+00	2.8E-03	1.1E-06	2.8E-05	1.7E-04		5.8E-04	0.0E+00
Br	0.0E+00	1.5E-05	0.0E+00	2.9E-04	1.2E-05	0.0E+00	1.4E-03	2.9E-05	3.8E-04	0.0E+00
Sn	0.0E+00	2.5E-05	0.0E+00	1.3E-04	2.8E-05	0.0E+00	3.8E-04	1.2E-05	0.0E+00	0.0E+00
Sb	0.0E+00	1.9E-05	0.0E+00	8.1E-06	3.2E-05	1.3E-04	8.2E-04	1.6E-04	0.0E+00	1.1E-03
Ba	0.0E+00	3.5E-04	0.0E+00	3.9E-03	7.9E-04	0.0E+00	2.8E-03	6.5E-04	0.0E+00	0.0E+00
Pb	0.0E+00	1.0E-06	0.0E+00	1.2E-04	2.2E-04	0.0E+00	2.1E-03	9.9E-06	0.0E+00	2.5E-04

	NRO	**ODE**	**OGA**	ORO	OTH	RAL	RWC	SHP	SOL
OC	2.1E-01	4.4E-01	5.9E-01	2.1E-01	1.1E-01	1.8E-01	4.2E-01	1.1E-01	2.7E-01
NO_3	1.3E-02	2.2E-02	1.6E-02	1.6E-03	9.2E-03	1.1E-03	7.8E-04	2.1E-08	3.6E-04
NH_4	1.7E-03	8.9E-03	1.7E-02	7.4E-05	7.2E-03	4.8E-09	6.1E-04	2.6E-09	7.5E-04
SO_4	2.9E-01	1.9E-02	3.7E-02	3.3E-02	1.4E-01	3.0E-03	4.0E-02	3.3E-01	2.8E-02
EC	9.3E-02	4.8E-01	2.8E-01	7.9E-02	2.6E-02	7.7E-01	4.5E-02	4.9E-02	4.7E-03
Na	8.1E-03	3.5E-03	1.9E-03	2.8E-04	3.8E-02	2.3E-08	1.3E-03	1.3E-08	2.4E-05
Al	8.3E-04	1.1E-03	9.1E-04	1.1E-03	1.3E-02	2.4E-09	4.5E-05	1.3E-09	2.5E-02
Si	1.1E-03	5.3E-03	3.2E-02	6.4E-02	3.8E-02	6.5E-08	8.0E-02	3.5E-03	2.5E-02
Cl	1.6E-02	3.0E-04	1.8E-03	3.2E-03	2.1E-02	2.1E-04	4.4E-03	1.8E-03	3.2E-03
K	6.5E-04	8.7E-04	6.4E-04	2.4E-04	1.7E-02	3.8E-05	5.6E-02	1.7E-04	2.0E-03
Ca	4.2E-03	4.1E-03	8.0E-03	7.6E-03	2.6E-02	5.8E-04	3.8E-03	2.9E-04	2.5E-02
Ti	7.3E-04	2.2E-04	9.5E-05	2.7E-03	4.3E-03	4.0E-06	0.0E+00	3.6E-04	1.7E-01
Mn	9.6E-05	5.1E-05	4.5E-05	8.1E-04	4.9E-04	2.2E-10	0.0E+00	2.1E-05	0.0E+00
Fe	5.2E-04	3.2E-03	3.4E-03	8.5E-02	8.0E-03	2.6E-04	3.7E-05	5.6E-04	3.3E-04
Cu	0.0E+00	1.0E-04	4.6E-04	8.5E-03	2.3E-04	0.0E+00	0.0E+00	8.7E-05	1.5E-05
Zn	9.5E-05	1.7E-03	5.3E-03	2.7E-03	6.8E-04	6.8E-04	9.0E-05	7.1E-04	1.1E-05
As	2.4E-07	1.7E-05	8.8E-06	7.3E-06	3.5E-05	3.0E-06	8.2E-07	0.0E+00	0.0E+00
Se	2.6E-04	1.7E-05	1.4E-05	2.0E-05	3.0E-05	6.7E-10	0.0E+00	2.8E-05	0.0E+00
Br	1.5E-04	2.9E-05	2.1E-04	3.3E-05	4.3E-04	1.5E-05	8.2E-06	2.4E-10	9.9E-05
Sn	2.0E-06	5.7E-05	1.2E-04	4.8E-03	7.9E-05	2.5E-05	4.1E-06	0.0E+00	0.0E+00
Sb	1.3E-04	1.7E-04	5.5E-04	0.0E+00	1.5E-04	1.9E-05	0.0E+00	1.3E-04	4.7E-03
Ba	2.8E-05	1.5E-03	1.8E-03	2.5E-02	6.2E-04	3.5E-04	0.0E+00	0.0E+00	1.3E-02
Pb	3.3E-07	7.6E-05	2.4E-04	8.0E-05	2.2E-04	1.0E-06	2.5E-06	0.0E+00	3.0E-04

Table S-3 Locations and CSN information for study sites. Population data is current as of the 2020 United States census.

Site Name	State	AQS Site ID	Latitude	Longitude	Elevation (m)[2]	Population[3]
Bakersfield	CA	06-029-0014	35.356092	-119.041209	123	403,455
Boise	ID	16-001-0010	43.600699	-116.3478530	823	235,684
Bountiful	UT	49-011-0004	40.902967	-111.8844670	1333	45,762
Denver	CO	08-031-0002	39.7511840	-104.9876250	1611	715,552
Fresno	CA	06-019-0011	36.785322	-119.774174	95	542,107
Hawthorne	UT	49-035-3006	40.736389	-111.8722220	1293	199,723
Las Vegas	NV	32-003-0540	36.1415384	-115.0820978	718	641,903
Modesto	CA	06-099-0005	37.642165	-120.9942120	27	218,464
Reno	NV	32-031-0016	39.525083	-119.8077170	1500	264,165
Sacramento	CA	06-067-0006	38.613779	-121.368014	8	524,943
Visalia	CA	06-107-2002	36.332179	-119.291228	97	141,384

Table S-4 Site-specific PCAP determinations during the study period. Omitted days did not have CSN observations at any site.

Date	BAK	BOI	BOU	DEN	FNO	HAW	LAS	MOD	REN	SAC	VIS
1/1/2016	Yes	Yes	Yes	Yes	Yes	Yes	Yes	No	Yes	No	No
1/4/2016	No	Yes	Yes	Yes	Yes	Yes	Yes	Yes	Yes	Yes	Yes
1/7/2016	No	No	Yes	No	No	Yes	No	No	No	No	No
1/10/2016	No	No	Yes	Yes	No	Yes	No	No	No	No	Yes
1/13/2016	Yes	Yes	Yes	Yes	Yes	Yes	Yes	Yes	Yes	Yes	Yes
1/16/2016	Yes	No	No	No	Yes	No	No	Yes	Yes	Yes	Yes
1/19/2016	Yes	No	No	No	Yes	No	No	No	No	No	No
1/22/2016	No	Yes	Yes	Yes	Yes	Yes	Yes	Yes	Yes	Yes	Yes
1/25/2016	Yes	No	No	No	Yes	No	No	No	No	No	Yes
1/28/2016	Yes	Yes	Yes	No	Yes	Yes	Yes	Yes	Yes	Yes	Yes
1/31/2016	Yes	No	Yes	No	Yes	Yes	No	No	No	No	No

Table S-5 Source categories used in nonlinear optimization.

Category name	**Description of included sources**
AG	Agricultural activities and livestock operations
AIR	Aircraft operations
BIO	Biogenics
COA	Coal combustion
DUS	Dust
FOI	Fuel oil combustion
MET	Metals processing
NDE	Non-road diesel combustion
NG	Natural gas combustion
NGA	Non-road gasoline
NRO	Non-road combustion of other fuels
ODE	On-road diesel combustion
OGA	On-road gasoline combustion
ORO	On-road combustion of other fuels
OTH	All other sources
RAL	Rail operations
RWC	Residential wood combustion
SHP	Marine shipping operations
SOL	Solvent use

Table S-6 Weather Research and Forecasting (WRF) model specifications for meteorology input data used in CMAQ-DDM and CMAQ-ISAM simulations.

Feature	Option used
Model version	4.3.3
Cumulus parameterization	Kain-Fritsch (new Eta)
Shallow convection	No shallow convection
Microphysics	Thompson
Longwave radiation	Rapid Radiative Transfer Model
Shortwave radiation	Dudhia
Planetary boundary layer scheme	Asymmetric Convective Model 2
Surface layer scheme	Pleim
Land-surface scheme	Pleim-Xiu land-surface model
Land use	MODIS

Table S-7 CMAQ model specifications used for CMAQ-DDM and CMAQ-ISAM simulations.

Feature	Description and/or option used
Chemical mechanism	cb6r5_ae7_aq
Ocean chemistry	Ocean halogen chemistry and sea spray aerosol emissions
Lightning NOx	Self-defined
K_z Min	Minimum K_z in eddy diffusion
Pleim-Xiu	WRF Pleim-Xiu land-surface model
Ammonia bi-directional flux	Ammonia bi-directional flux for in-line deposition velocities
Surface HONO	Surface HONO interaction
Gravitational settling	Vertical diffusion aerosol gravitational sedimentation
Biogenic emissions	In-line biogenic emissions with BEIS
Surface tiled aerosol and gaseous exchange	Emerson et al., 2020[3] aerosol deposition model

Table S-8 Speciated $PM_{2.5}$ concentrations averaged across PCAPs and non-PCAPs at the ten study sites experiencing both conditions. Units are in μg m^{-3} for all data.

	Bakersfield		Boise		Bountiful		Denver		Fresno	
PCAP?	**Yes**	**No**	**Yes**	**No**	**Yes**	**No**	**Yes**	**No**	**Yes**	**No**
OC	6.61	2.42	2.21	2.40	1.92	0.81	3.41	2.05	4.70	4.84
NO_3	10.89	1.96	3.98	2.57	7.87	2.27	4.42	2.38	4.81	3.26
NH_4	3.28	0.35	0.93	0.37	2.45	0.35	1.14	0.35	1.42	0.84
SO_4	1.39	0.54	0.45	0.25	1.43	0.50	0.92	0.43	0.79	0.54
EC	1.92	0.75	0.75	0.64	0.68	0.35	1.17	0.87	1.17	1.24
Na	0.01	0.03	0.02	0.01	0.07	0.02	0.07	0.07	0.01	0.05
Al	0.02	0.01	0.02	0.01	0.02	0.00	0.04	0.08	0.00	0.01
Si	0.08	0.05	0.05	0.09	0.05	0.02	0.12	0.23	0.04	0.02
Cl	0.41	0.02	0.04	0.01	0.13	0.00	0.07	0.07	0.02	0.11
K	0.34	0.05	0.07	0.05	0.24	0.01	0.22	0.06	0.13	0.24
Ca	0.05	0.03	0.03	0.04	0.05	0.02	0.07	0.09	0.03	0.02
Ti	0.01	0.00	0.00	0.00	0.00	0.00	0.01	0.01	0.00	0.00
Mn	0.00	0.00	0.00	0.00	0.00	0.00	0.00	0.00	0.00	0.00
Fe	0.12	0.10	0.06	0.06	0.06	0.05	0.14	0.15	0.09	0.05
Cu	0.01	0.01	0.01	0.00	0.01	0.00	0.01	0.01	0.01	0.01
Zn	0.03	0.01	0.02	0.01	0.03	0.01	0.02	0.01	0.01	0.02
As	0.00	0.00	0.00	0.00	0.00	0.00	0.00	0.00	0.00	0.00
Se	0.00	0.00	0.00	0.00	0.00	0.00	0.00	0.00	0.00	0.00
Br	0.01	0.00	0.00	0.00	0.01	0.00	0.00	0.00	0.00	0.00
Sn	0.01	0.00	0.00	0.01	0.01	0.00	0.01	0.01	0.00	0.01
Sb	0.02	0.02	0.01	0.00	0.02	0.00	0.01	0.01	0.00	0.00
Ba	0.03	0.02	0.05	0.01	0.02	0.02	0.02	0.02	0.03	0.05
Pb	0.01	0.01	0.01	0.00	0.00	0.00	0.01	0.00	0.01	0.01

	Hawthorne		Las Vegas		Modesto		Reno		Sacramento	
PCAP?	**Yes**	**No**	**Yes**	**No**	**Yes**	**No**	**Yes**	**No**	**Yes**	**No**
OC	2.30	0.93	5.69	1.70	3.40	2.18	2.32	1.61	3.94	3.89
NO_3	7.05	2.25	1.80	0.69	5.86	2.28	1.61	1.33	3.03	1.19
NH_4	1.58	0.42	0.13	0.02	1.88	0.52	0.26	0.10	0.67	0.09
SO_4	0.78	0.28	0.38	0.17	1.01	0.54	0.19	0.13	0.58	0.27
EC	0.93	0.45	1.79	0.49	0.45	0.45	0.84	0.58	1.09	0.98
Na	0.04	0.01	0.00	0.01	0.40	0.40	0.02	0.02	0.07	0.07
Al	0.02	0.00	0.04	0.04	0.01	0.01	0.03	0.01	0.00	0.00
Si	0.08	0.02	0.15	0.14	0.03	0.02	0.09	0.05	0.03	0.02
Cl	0.19	0.01	0.03	0.01	0.57	0.04	0.01	0.01	0.01	0.02
K	0.14	0.02	0.21	0.07	0.11	0.13	0.07	0.04	0.13	0.13
Ca	0.08	0.04	0.27	0.14	0.03	0.02	0.04	0.02	0.02	0.01
Ti	0.01	0.00	0.02	0.01	0.00	0.00	0.01	0.00	0.00	0.00
Mn	0.00	0.00	0.01	0.00	0.00	0.00	0.00	0.00	0.00	0.00
Fe	0.11	0.05	0.21	0.09	0.04	0.02	0.07	0.03	0.06	0.04
Cu	0.01	0.00	0.02	0.00	0.00	0.01	0.00	0.00	0.00	0.02
Zn	0.02	0.01	0.02	0.01	0.05	0.01	0.01	0.00	0.01	0.01
As	0.00	0.00	0.00	0.00	0.00	0.00	0.00	0.00	0.00	0.00
Se	0.00	0.00	0.00	0.00	0.00	0.00	0.00	0.00	0.00	0.00
Br	0.01	0.00	0.01	0.00	0.00	0.00	0.00	0.00	0.00	0.00
Sn	0.00	0.00	0.01	0.00	0.04	0.03	0.01	0.01	0.00	0.01
Sb	0.00	0.00	0.02	0.01	0.01	0.01	0.01	0.00	0.00	0.01
Ba	0.03	0.00	0.04	0.02	0.01	0.02	0.01	0.01	0.01	0.00
Pb	0.00	0.00	0.01	0.01	0.00	0.00	0.01	0.00	0.01	0.01

Sensitivity outputs from CMAQ-DDM and CMAQ-ISAM

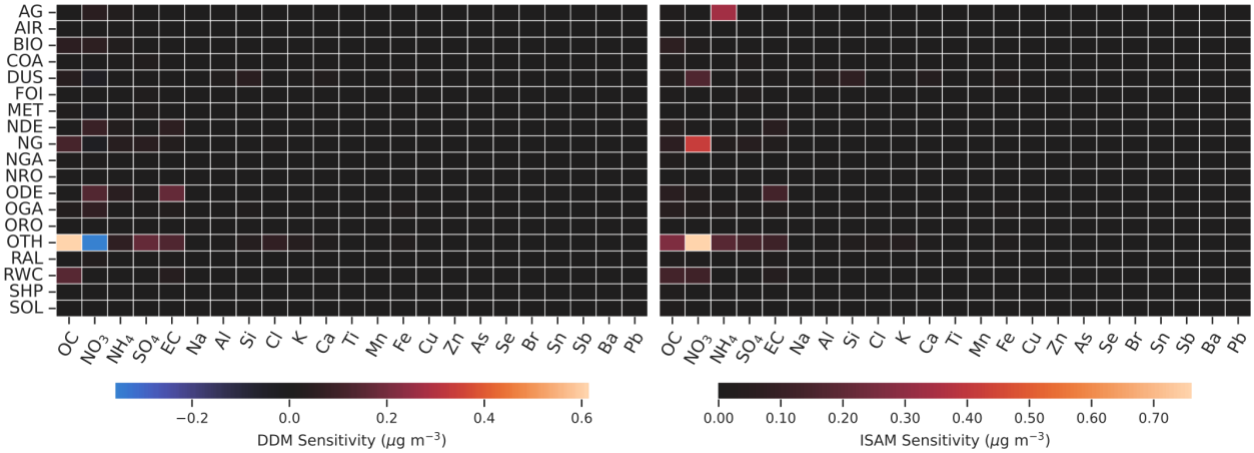

Figure S-1 BAK Sensitivities on January 1, 2016 from CMAQ-DDM (left) and CMAQ-ISAM (right).

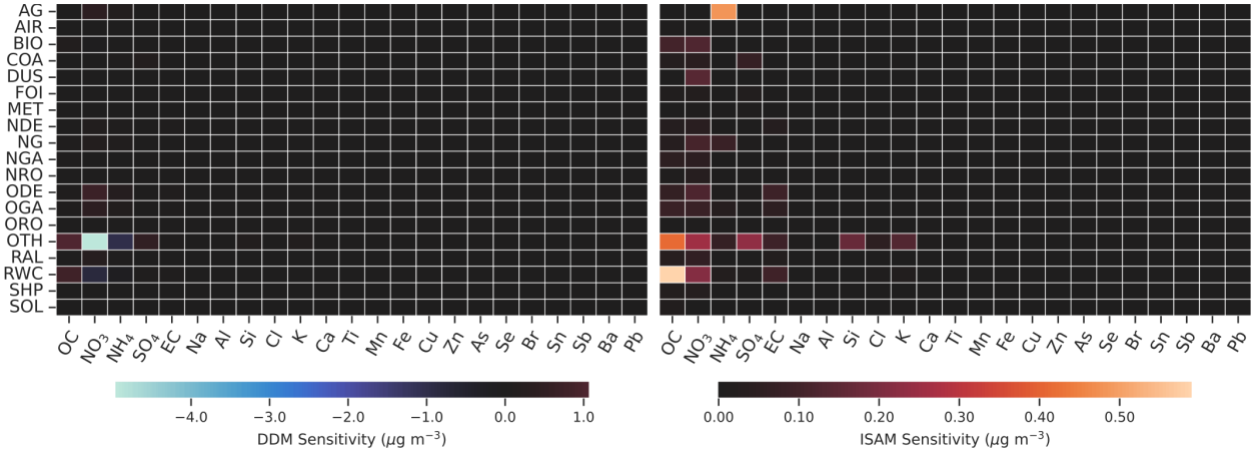

Figure S-2 BOI Sensitivities on January 1, 2016 from CMAQ-DDM (left) and CMAQ-ISAM (right).

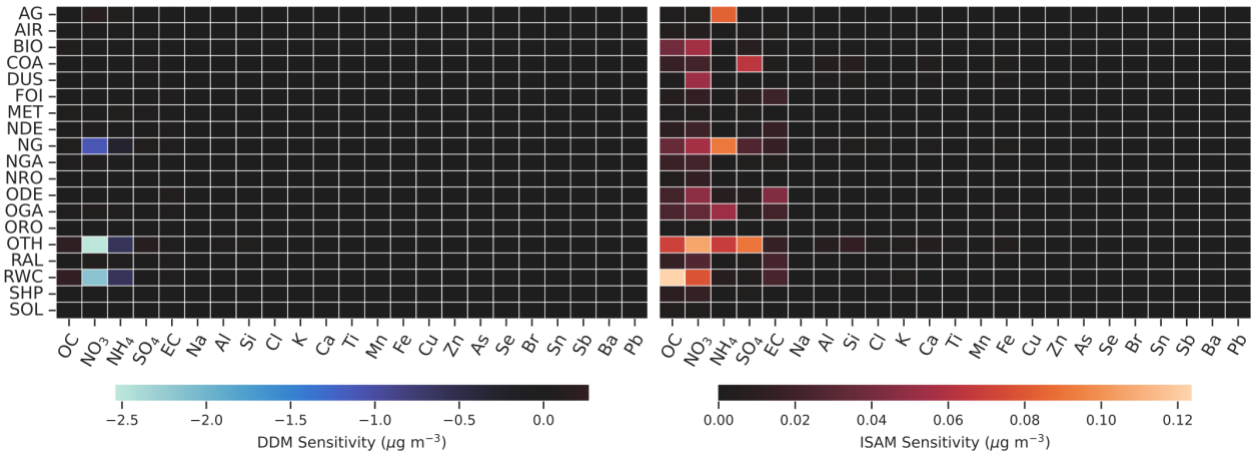

Figure S-3 BOU Sensitivities on January 1, 2016 from CMAQ-DDM (left) and CMAQ-ISAM (right).

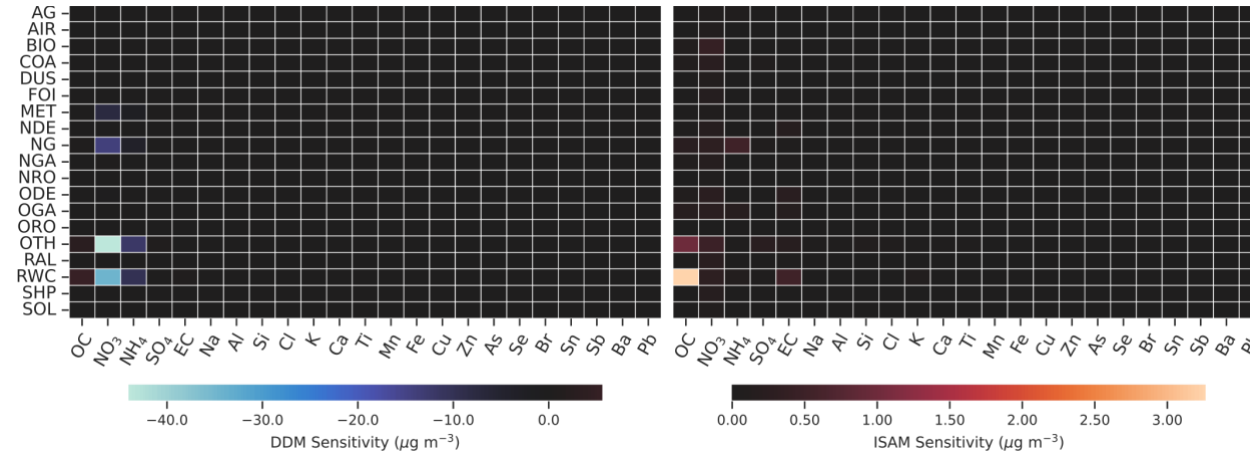

Figure S-4 DEN Sensitivities on January 1, 2016 from CMAQ-DDM (left) and CMAQ-ISAM (right).

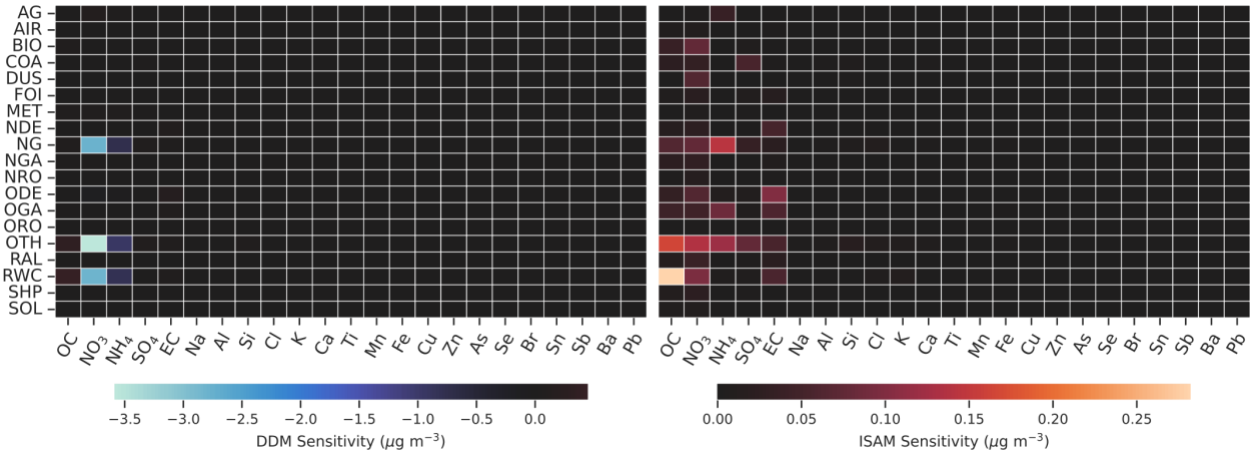

Figure S-5 FNO Sensitivities on January 1, 2016 from CMAQ-DDM (left) and CMAQ-ISAM (right).

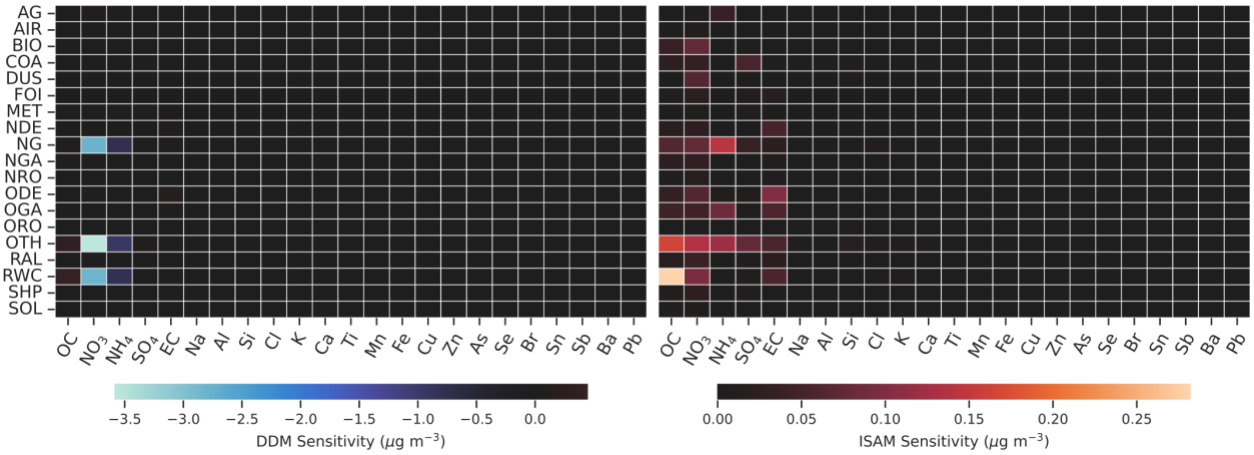

Figure S-6 HAW Sensitivities on January 1, 2016 from CMAQ-DDM (left) and CMAQ-ISAM (right).

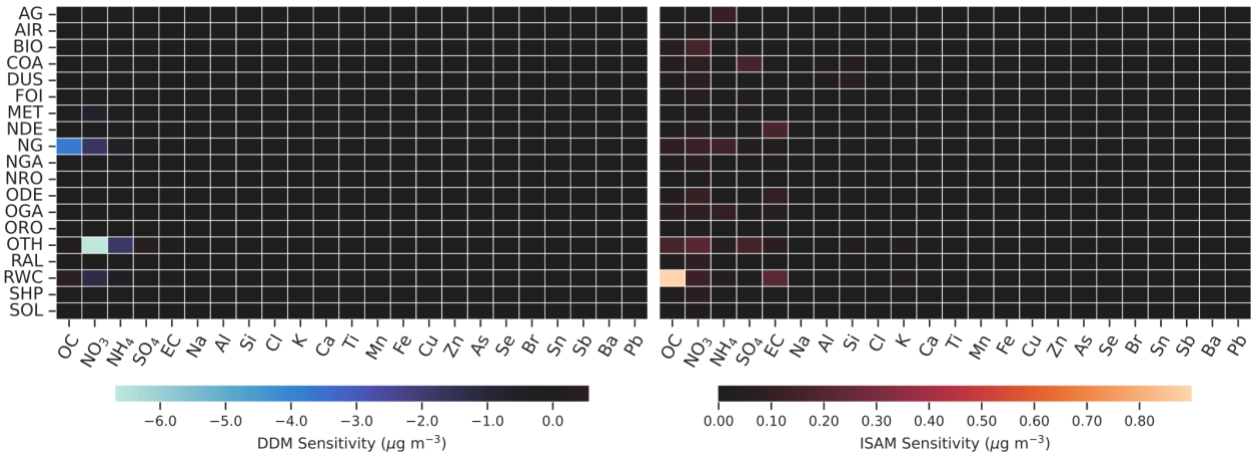

Figure S-7 LAS Sensitivities on January 1, 2016 from CMAQ-DDM (left) and CMAQ-ISAM (right).

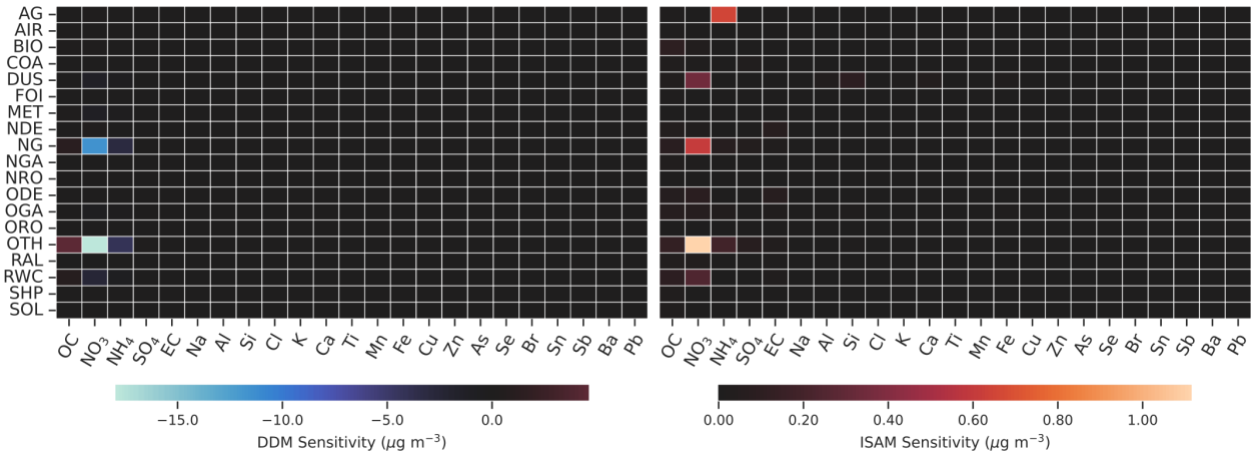

Figure S-8 MOD Sensitivities on January 1, 2016 from CMAQ-DDM (left) and CMAQ-ISAM (right).

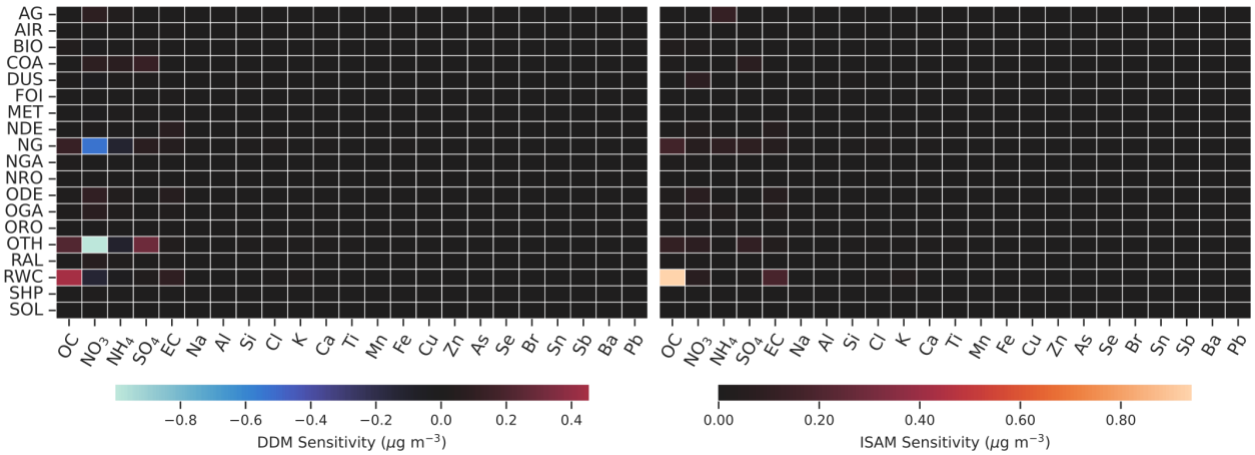

Figure S-9 REN Sensitivities on January 1, 2016 from CMAQ-DDM (left) and CMAQ-ISAM (right).

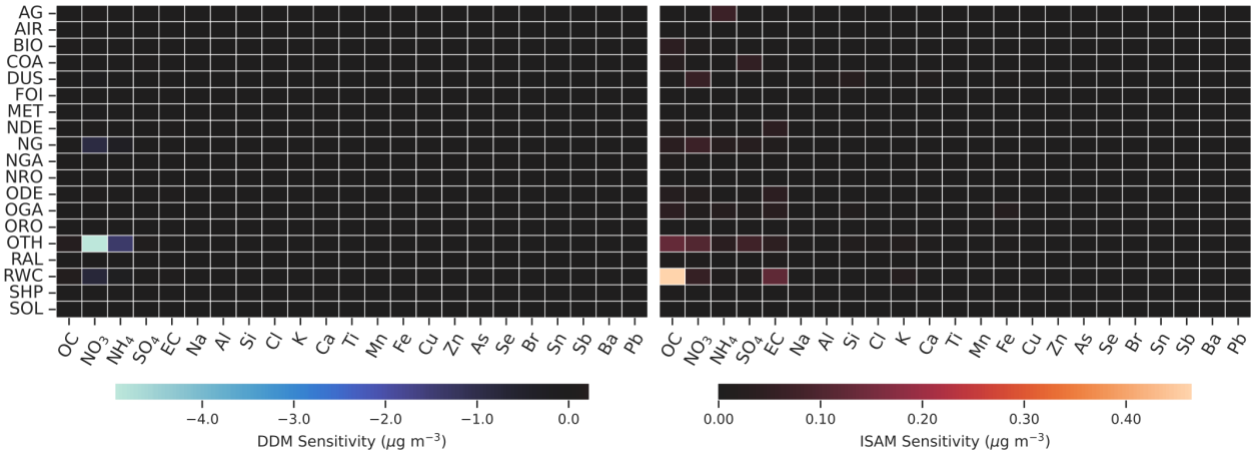

Figure S-10 SAC Sensitivities on January 1, 2016 from CMAQ-DDM (left) and CMAQ-ISAM (right).

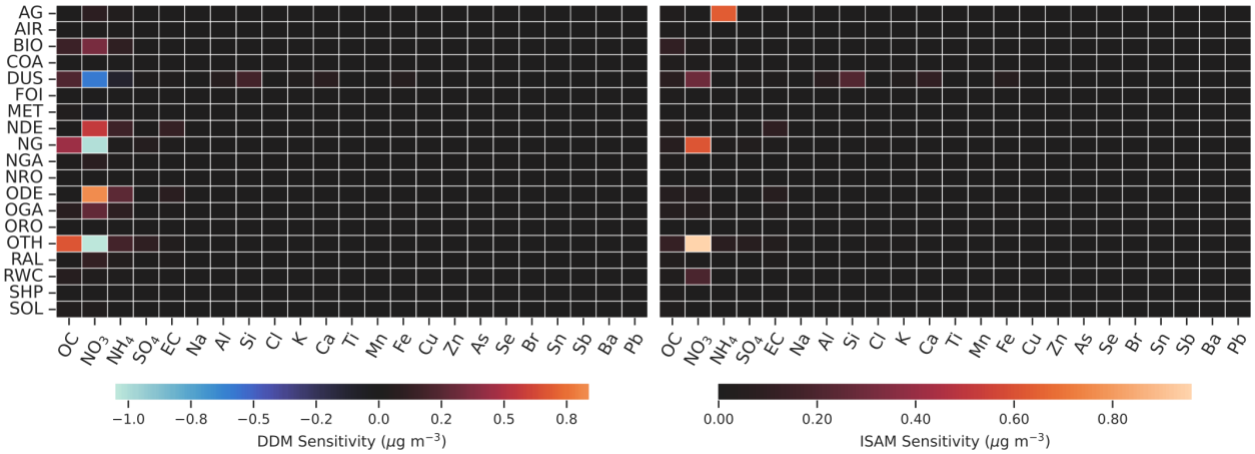

Figure S-11 VIS Sensitivities on January 1, 2016 from CMAQ-DDM (left) and CMAQ-ISAM (right).

Optimized profiles for January 1 using the standard seed profile

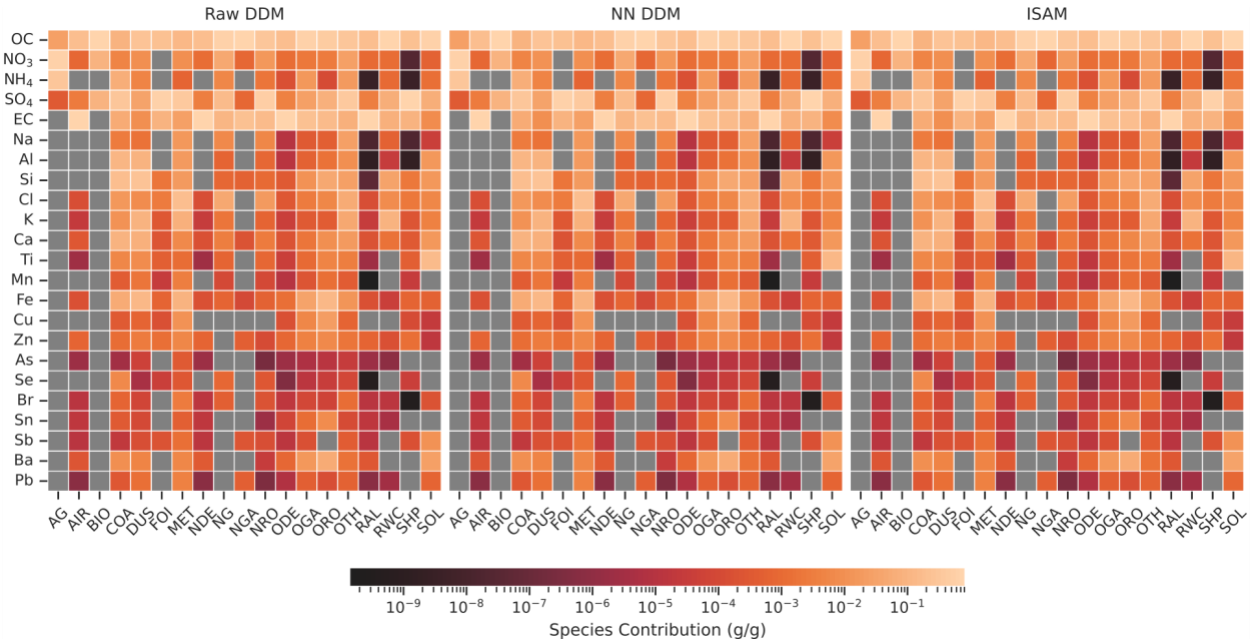

Figure S-12 BAK optimized profiles using raw DDM (left), positively constrained DDM (center), and ISAM (right) as sensitivity input data. Gray squares indicate that the optimization found no contribution of that species in that source.

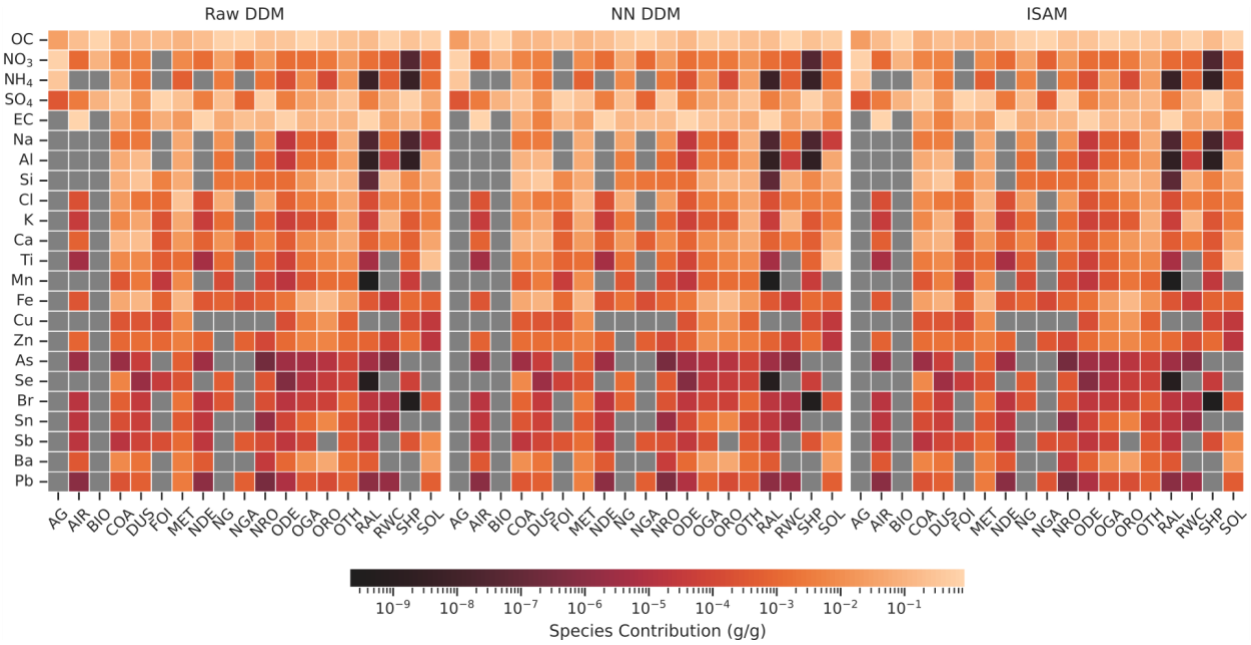

Figure S-13 BOI optimized profiles using raw DDM (left), positively constrained DDM (center), and ISAM (right) as sensitivity input data. Gray squares indicate that the optimization found no contribution of that species in that source.

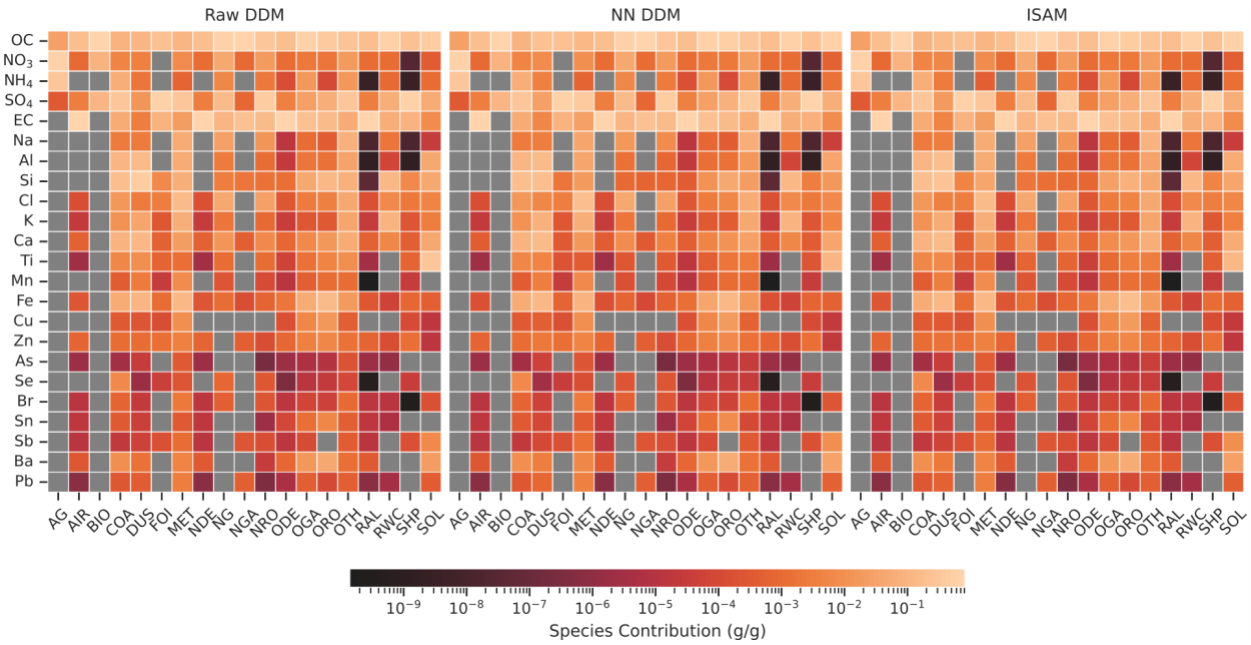

Figure S-14 BOU optimized profiles using raw DDM (left), positively constrained DDM (center), and ISAM (right) as sensitivity input data. Gray squares indicate that the optimization found no contribution of that species in that source.

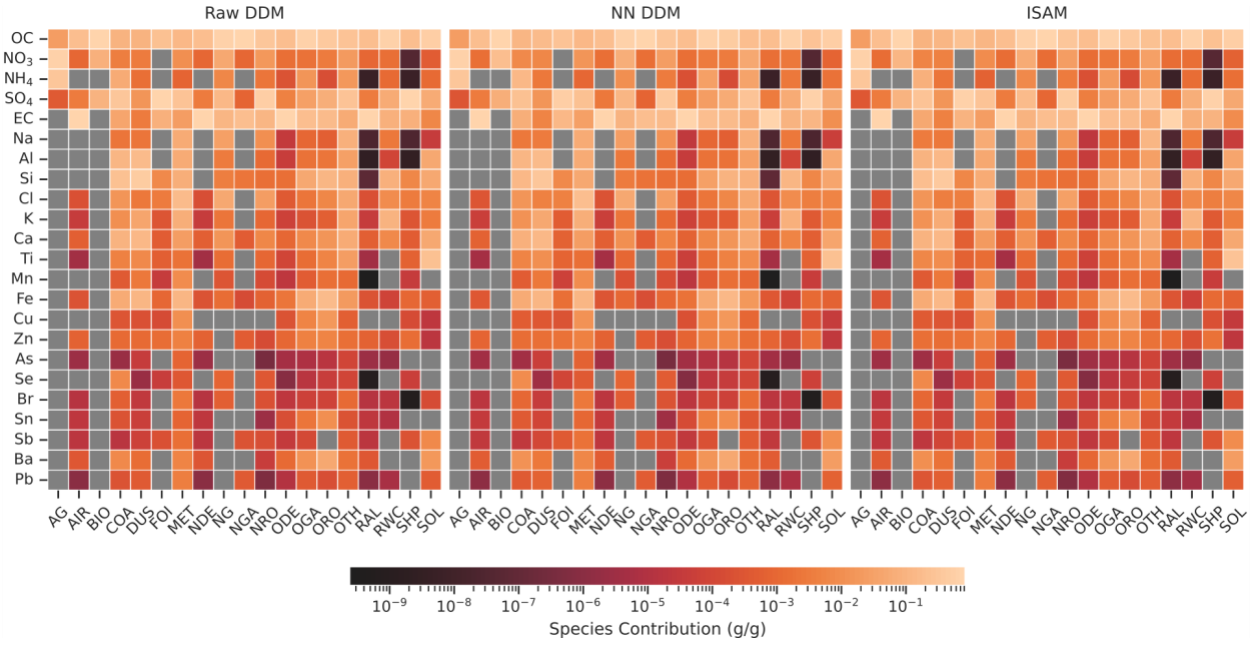

Figure S-15 DEN optimized profiles using raw DDM (left), positively constrained DDM (center), and ISAM (right) as sensitivity input data. Gray squares indicate that the optimization found no contribution of that species in that source.

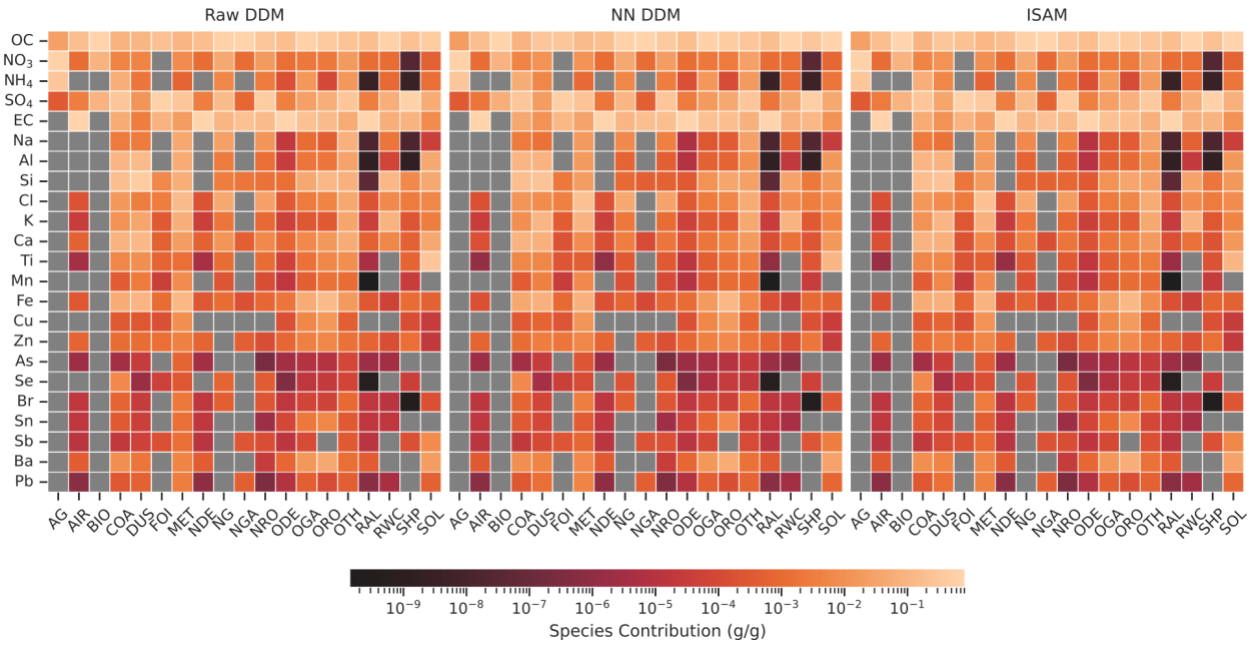

Figure S-16 FNO optimized profiles using raw DDM (left), positively constrained DDM (center), and ISAM (right) as sensitivity input data. Gray squares indicate that the optimization found no contribution of that species in that source.

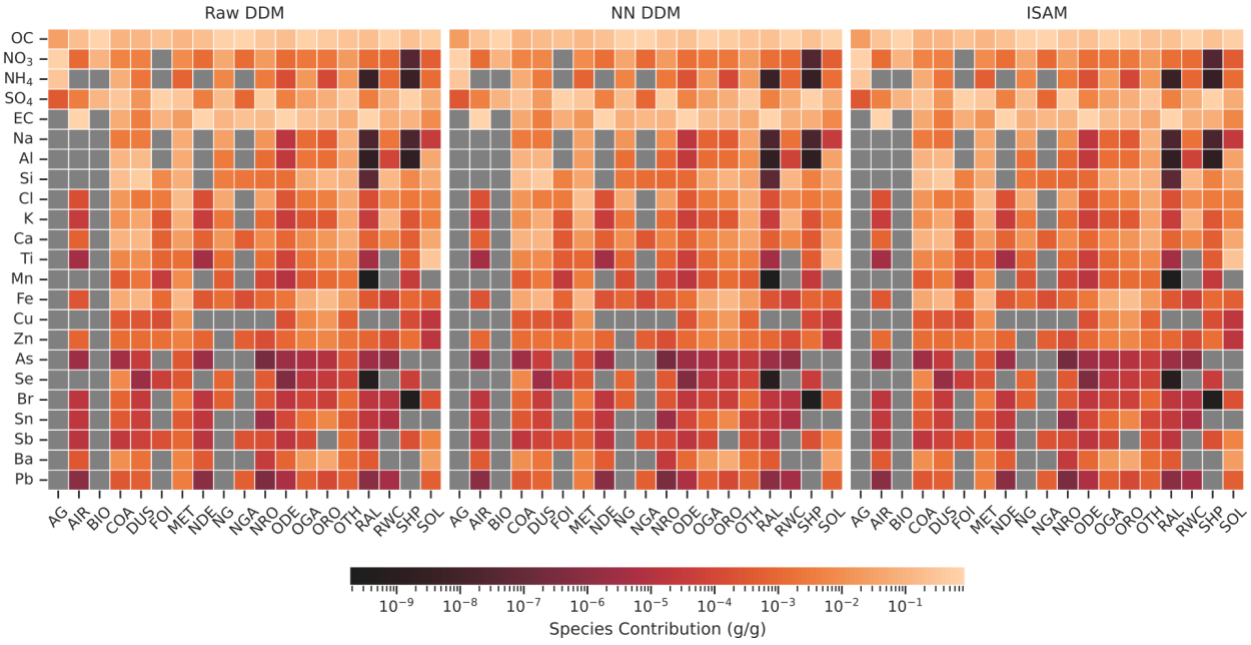

Figure S-17 HAW optimized profiles using raw DDM (left), positively constrained DDM (center), and ISAM (right) as sensitivity input data. Gray squares indicate that the optimization found no contribution of that species in that source.

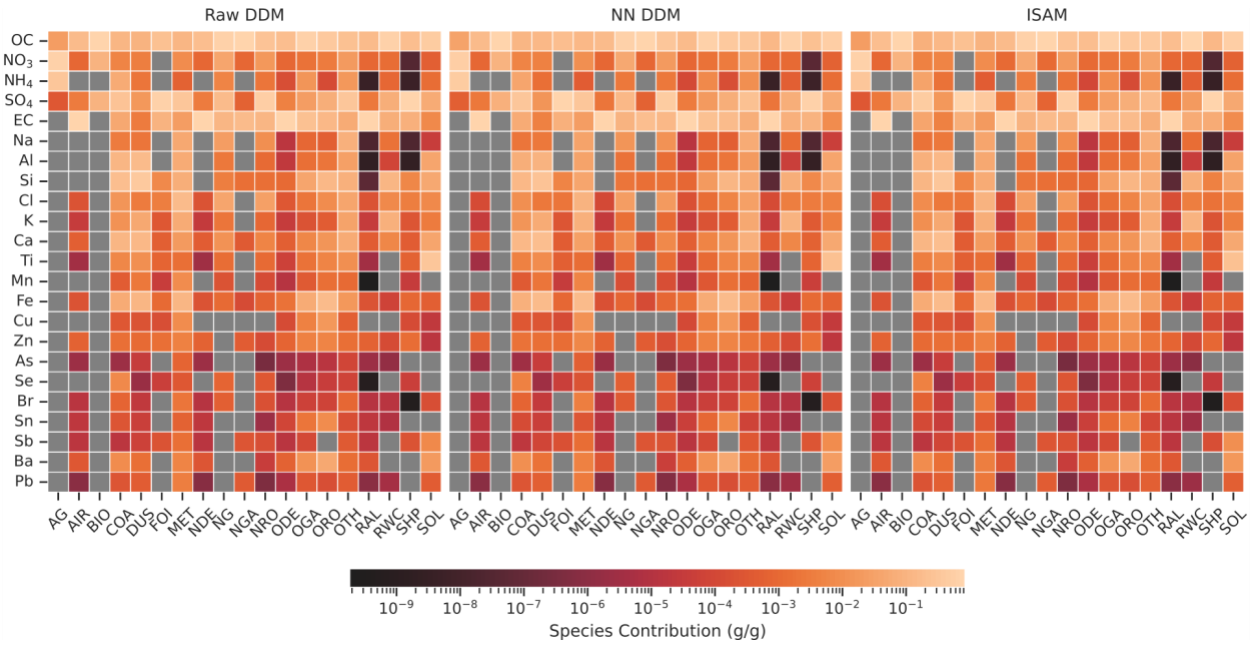

Figure S-18 LAS optimized profiles using raw DDM (left), positively constrained DDM (center), and ISAM (right) as sensitivity input data. Gray squares indicate that the optimization found no contribution of that species in that source.

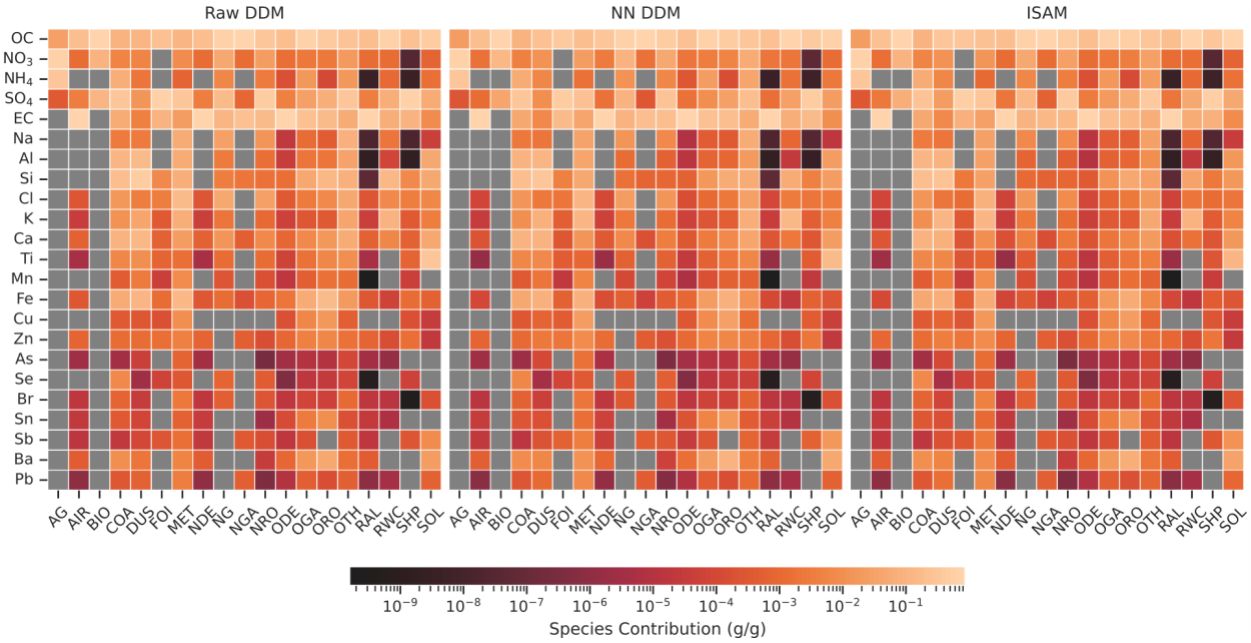

Figure S-19 MOD optimized profiles using raw DDM (left), positively constrained DDM (center), and ISAM (right) as sensitivity input data. Gray squares indicate that the optimization found no contribution of that species in that source.

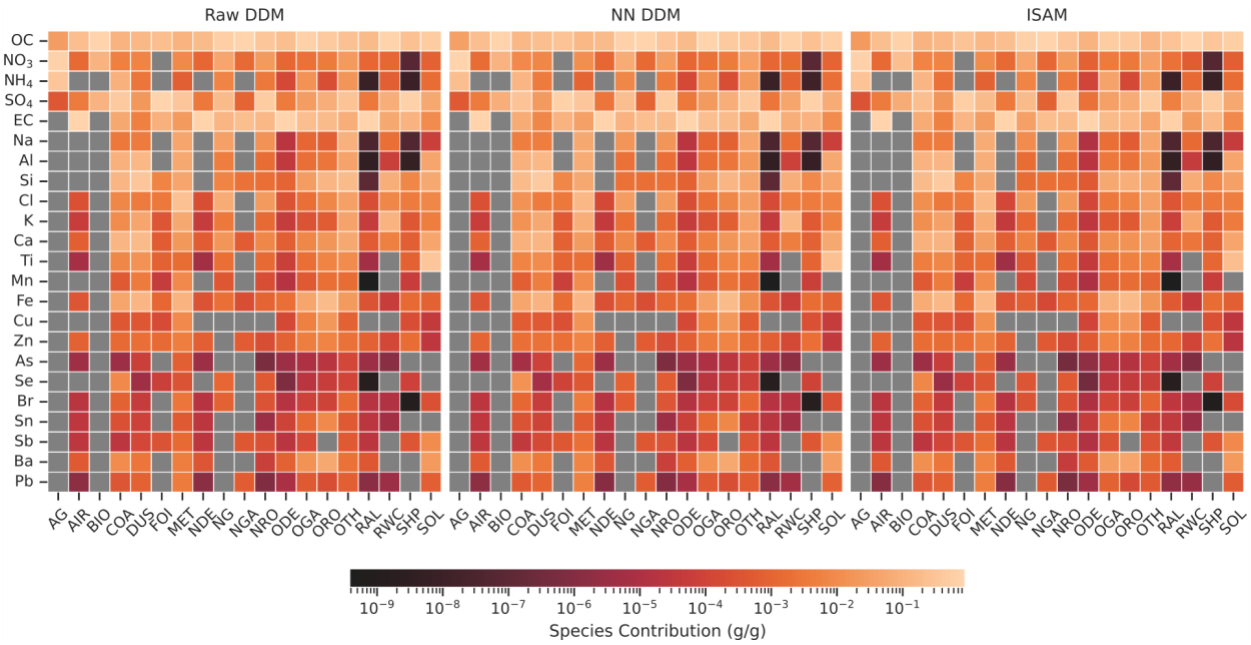

Figure S-20 REN optimized profiles using raw DDM (left), positively constrained DDM (center), and ISAM (right) as sensitivity input data. Gray squares indicate that the optimization found no contribution of that species in that source.

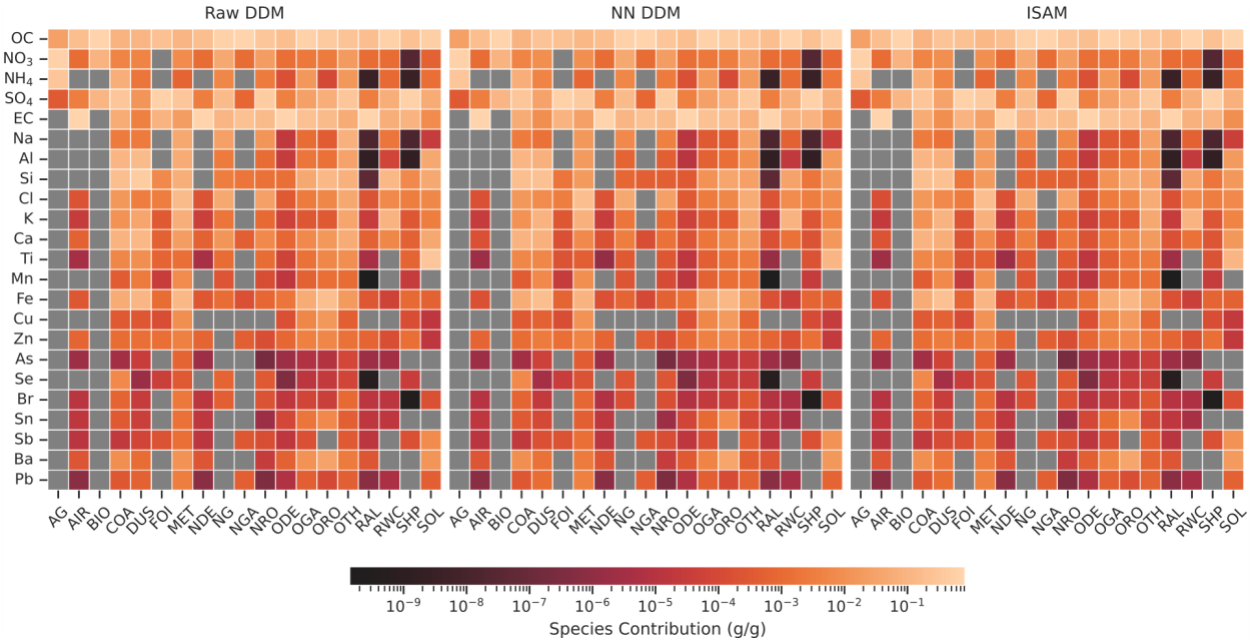

Figure S-21 SAC optimized profiles using raw DDM (left), positively constrained DDM (center), and ISAM (right) as sensitivity input data. Gray squares indicate that the optimization found no contribution of that species in that source.

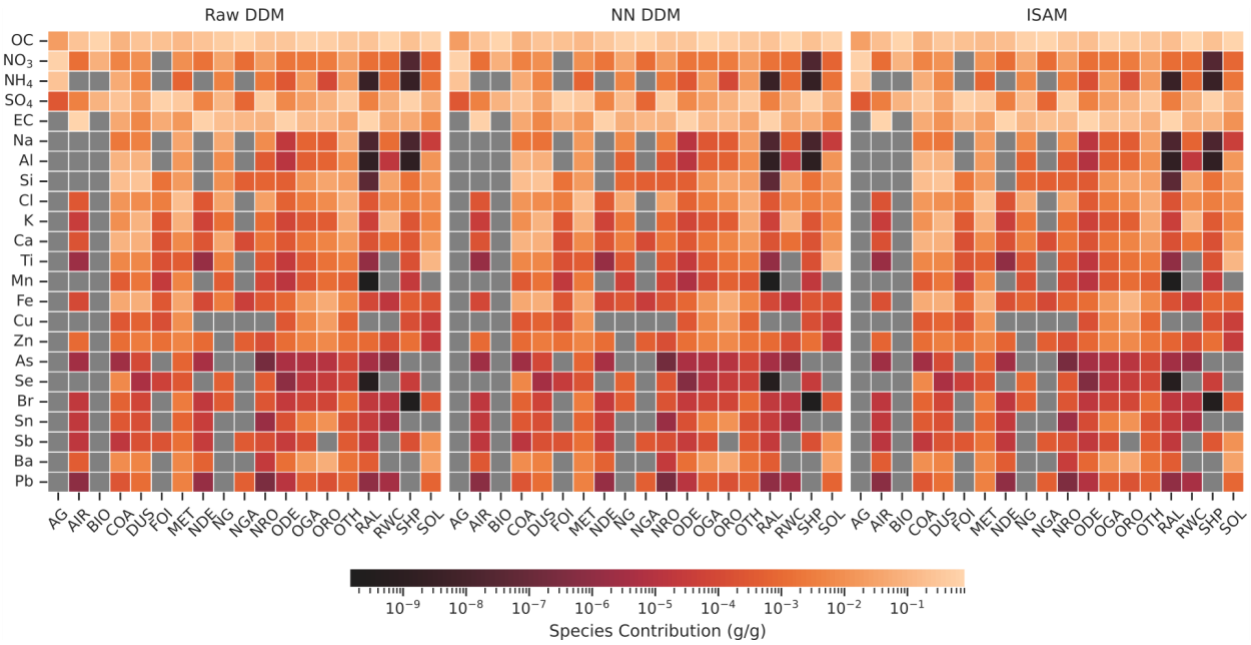

Figure S-22 VIS optimized profiles using raw DDM (left), positively constrained DDM (center), and ISAM (right) as sensitivity input data. Gray squares indicate that the optimization found no contribution of that species in that source.

Optimized ISAM PCAP and non-PCAP profiles using the standard seed

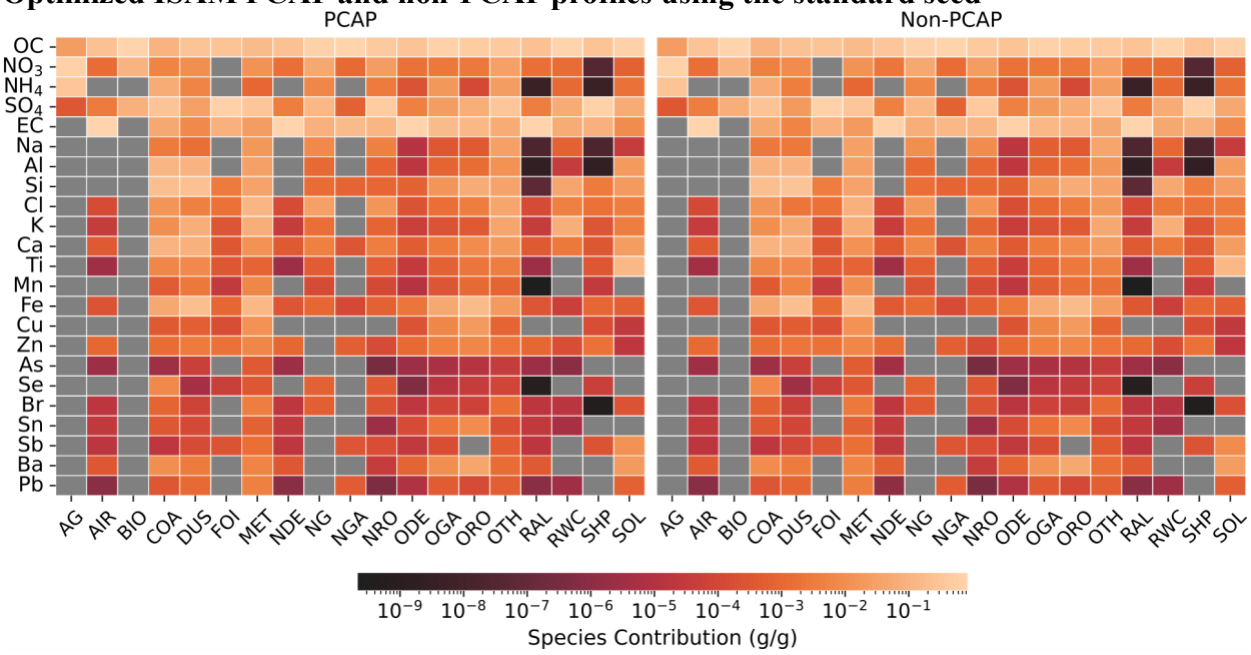

Figure S-23 BAK composite source profiles for PCAP (left) and non-PCAP (right) periods. Number of profiles used for the PCAP average profile = 4. Number of profiles used for the non-PCAP average profile = 3. Gray squares indicate that the species is not contributed by the source.

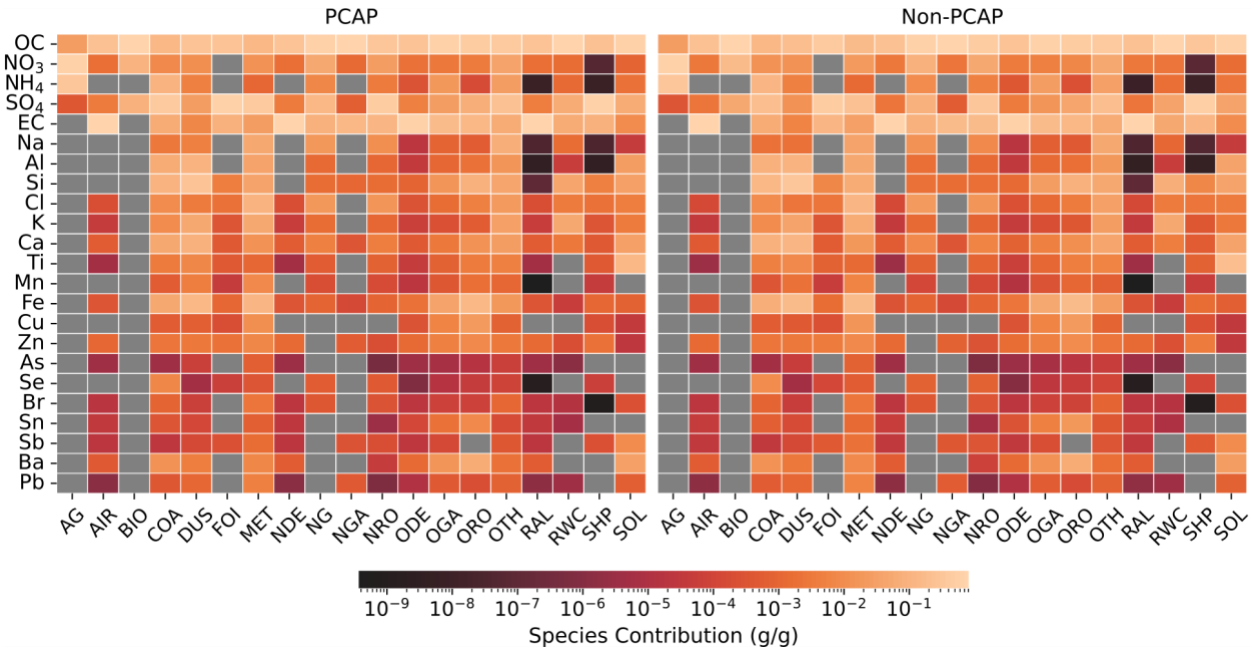

Figure S-24 BOI composite source profiles for PCAP (left) and non-PCAP (right) periods. Number of profiles used for the PCAP average profile = 5. Number of profiles used for the non-PCAP average profile = 3. Gray squares indicate that the species is not contributed by the source.

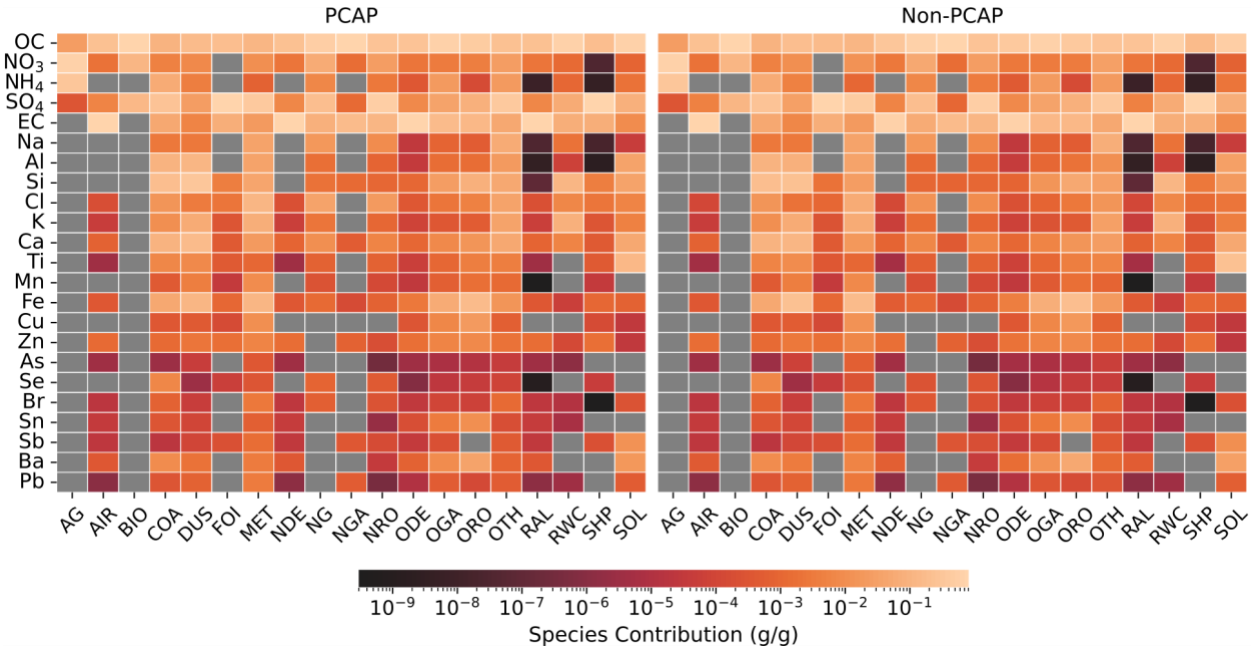

Figure S-25 BOU composite source profiles for PCAP (left) and non-PCAP (right) periods. Number of profiles used for the PCAP average profile = 4. Number of profiles used for the non-PCAP average profile =3. Gray squares indicate that the species is not contributed by the source.

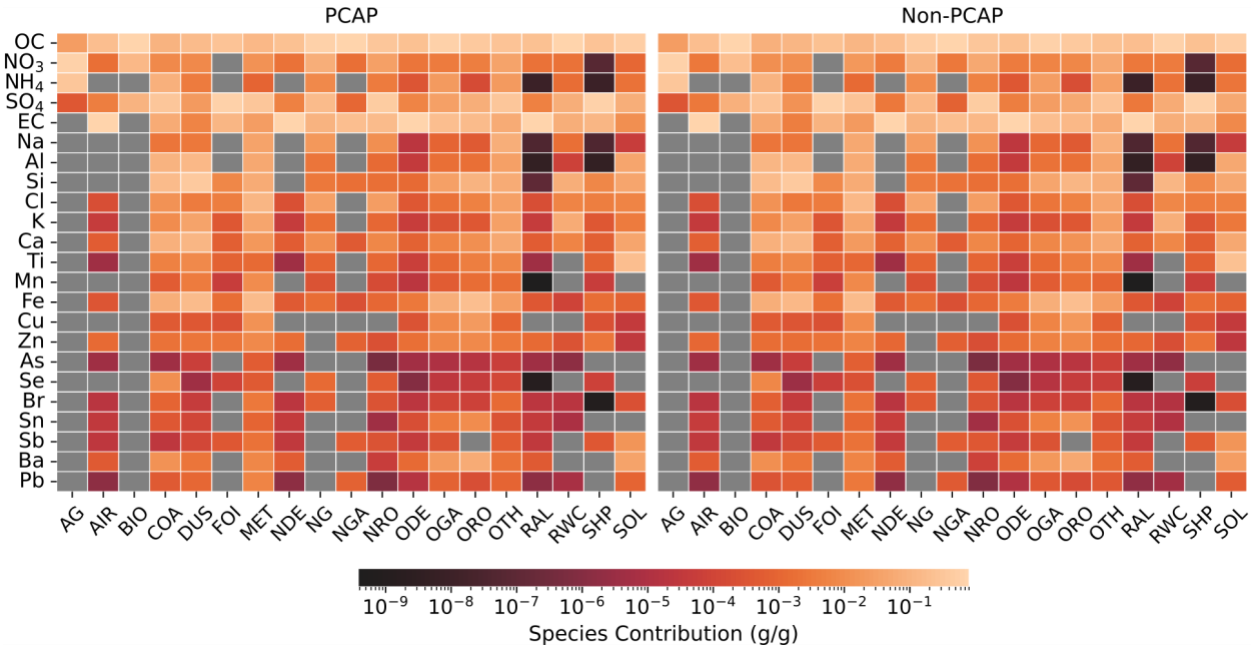

Figure S-26 DEN composite source profiles for PCAP (left) and non-PCAP (right) periods. Number of profiles used for the PCAP average profile = 3. Number of profiles used for the non-PCAP average profile= 5. Gray squares indicate that the species is not contributed by the source.

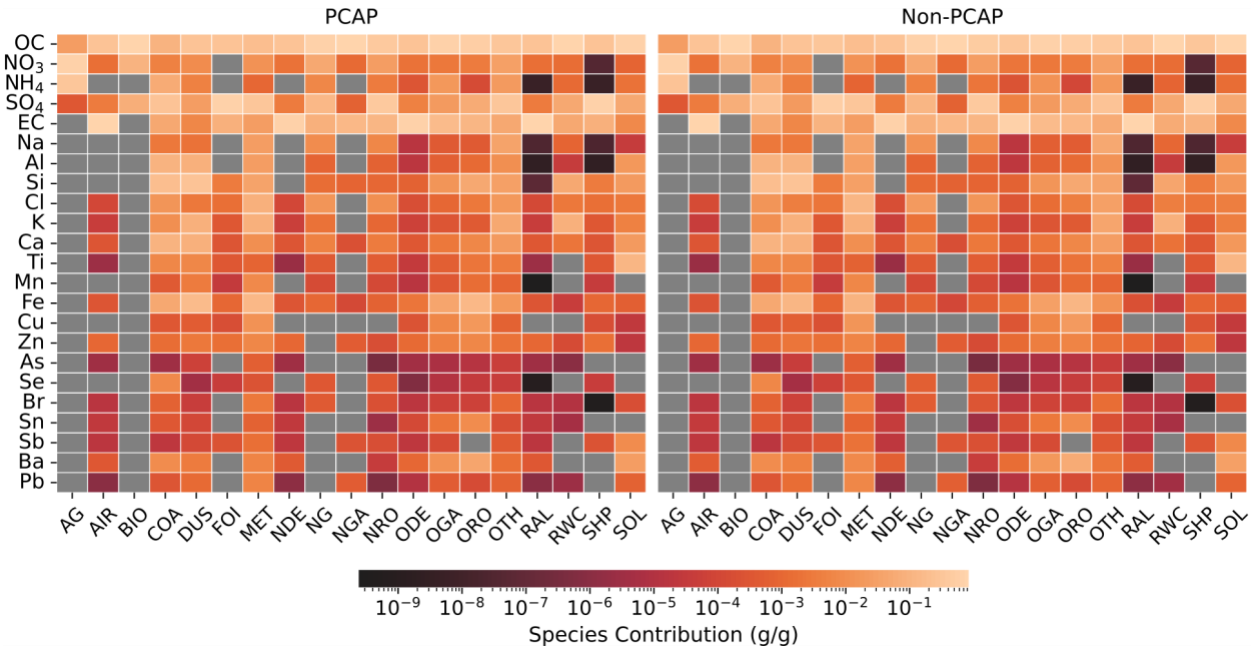

Figure S-27 FNO composite source profiles for PCAP (left) and non-PCAP (right) periods. Number of profiles used for the PCAP average profile = 5. Number of profiles used for the non-PCAP average profile = 6. Gray squares indicate that the species is not contributed by the source.

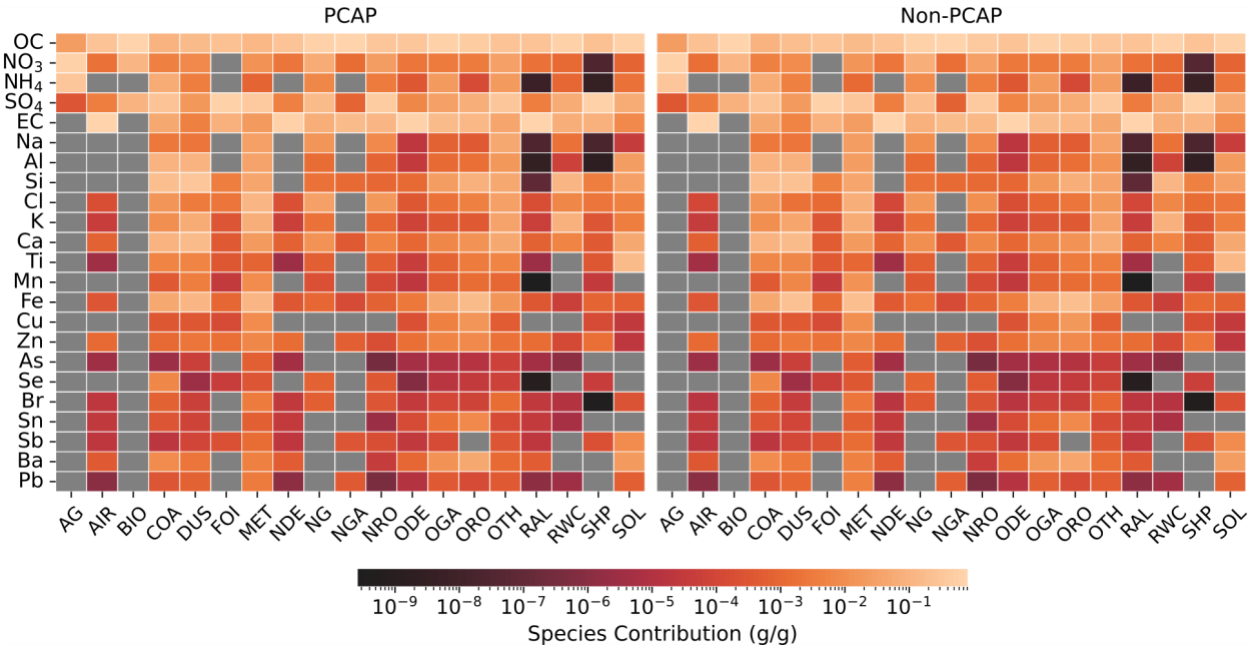

Figure S-28 HAW composite source profiles for PCAP (left) and non-PCAP (right) periods. Number of profiles used for the PCAP average profile = 6. Number of profiles used for the non-PCAP average profile = 2. Gray squares indicate that the species is not contributed by the source.

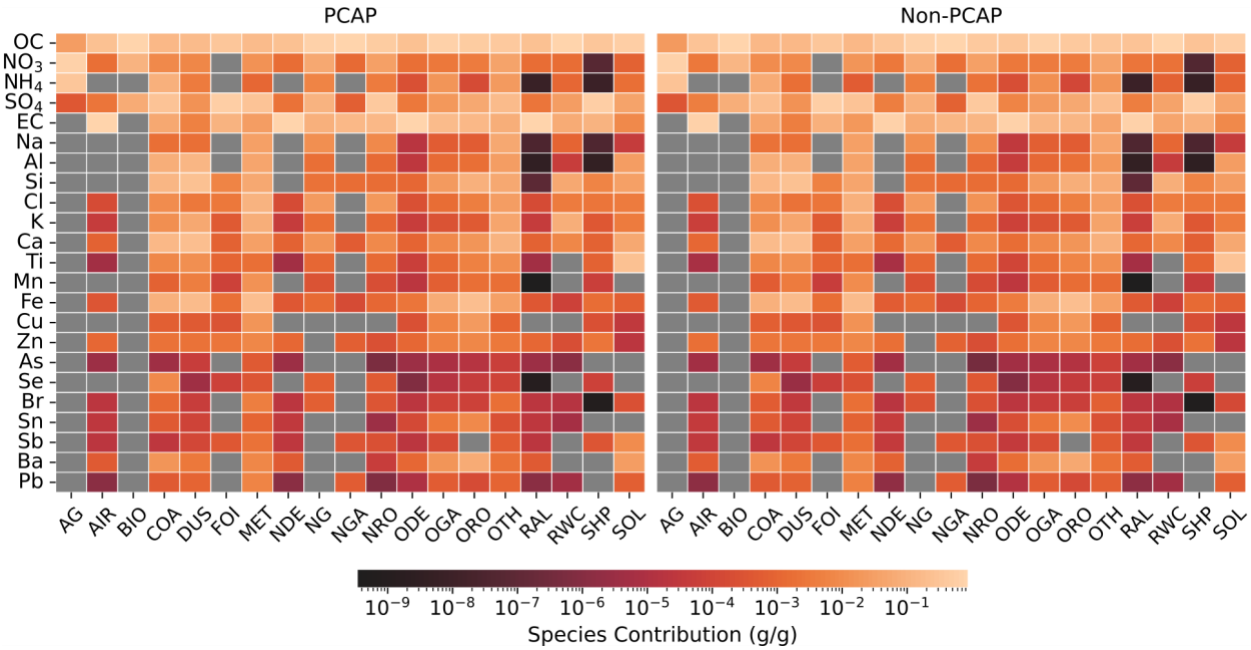

Figure S-29 LAS composite source profiles for PCAP (left) and non-PCAP (right) periods. Number of profiles used for the PCAP average profile = 3. Number of profiles used for the non-PCAP average profile = 5. Gray squares indicate that the species is not contributed by the source.

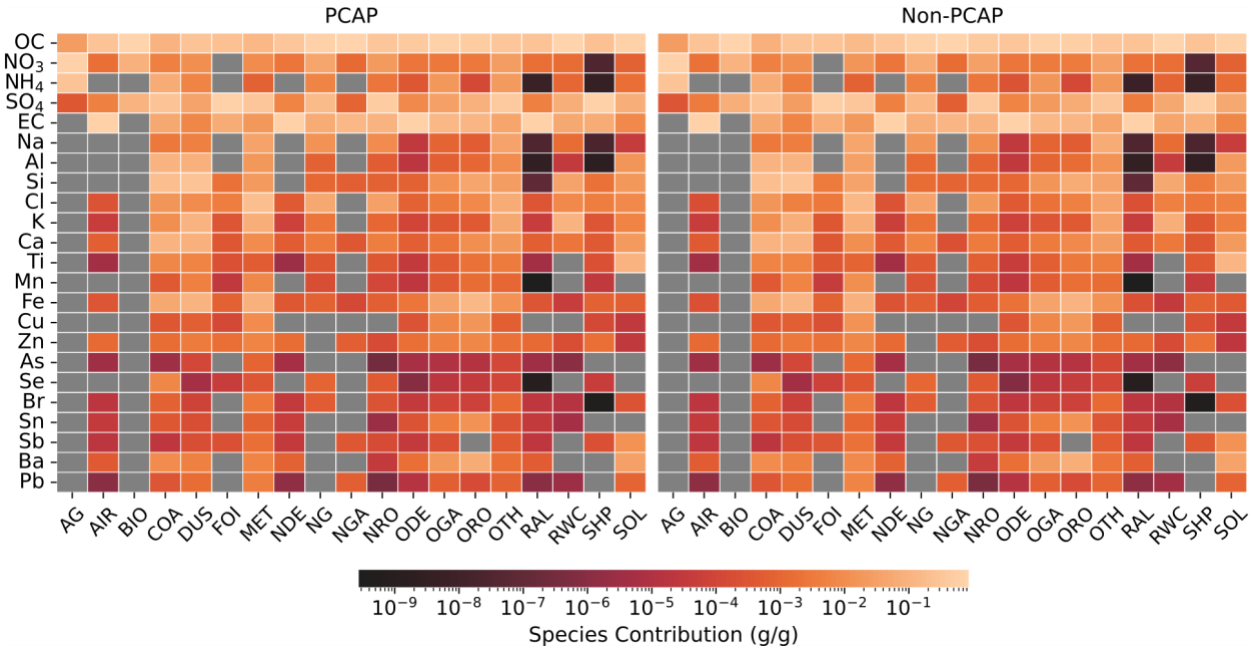

Figure S-30 MOD composite source profiles for PCAP (left) and non-PCAP (right) periods. Number of profiles used for the PCAP average profile = 1. Number of profiles used for the non-PCAP average profile = 4. Gray squares indicate that the species is not contributed by the source.

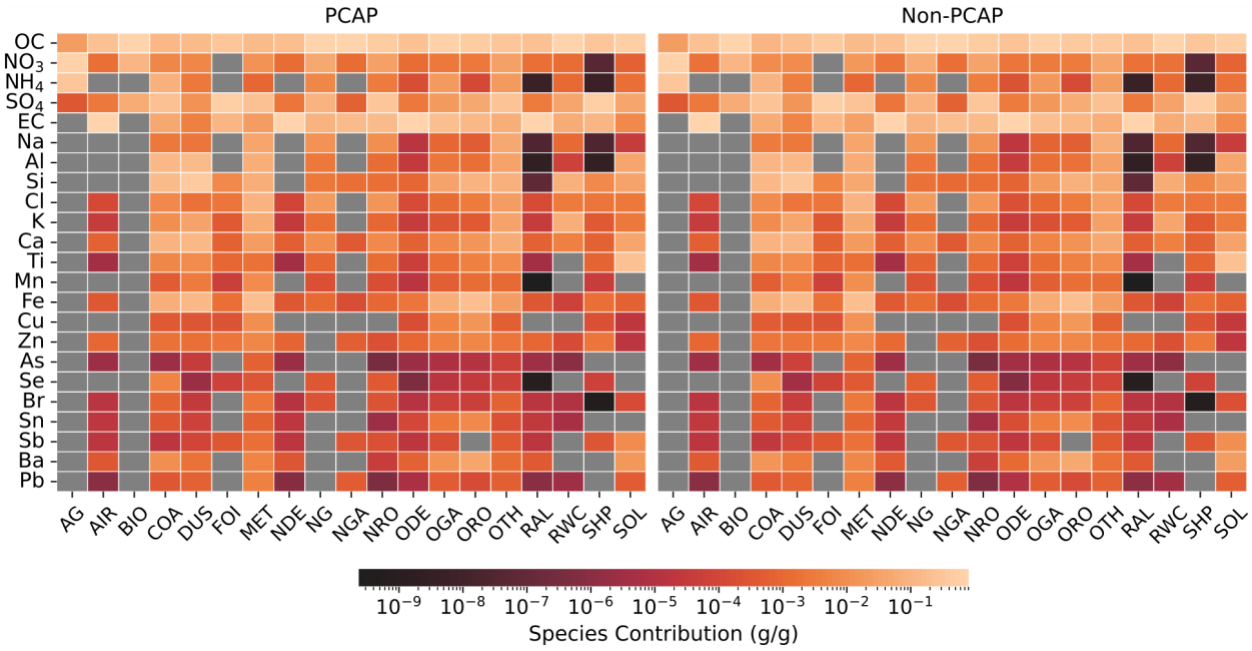

Figure S-31 REN composite source profiles for PCAP (left) and non-PCAP (right) periods. Number of profiles used for the PCAP average profile = 3. Number of profiles used for the non-PCAP average profile = 5. Gray squares indicate that the species is not contributed by the source.

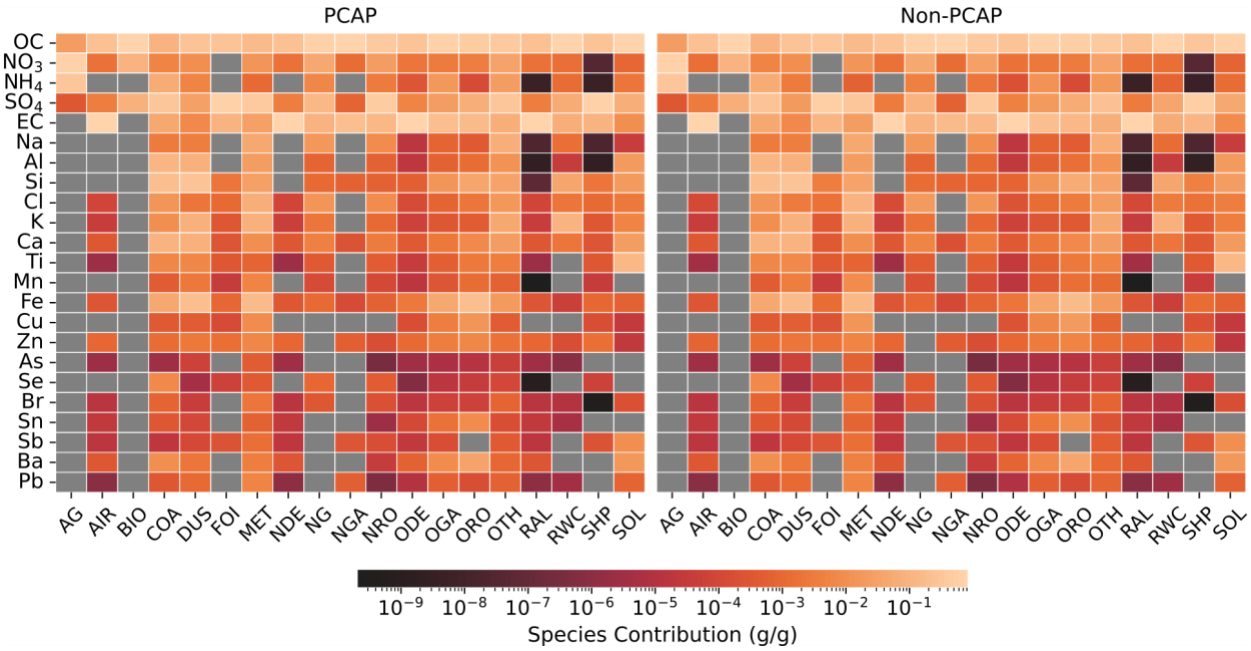

Figure S-32 SAC composite source profiles for PCAP (left) and non-PCAP (right) periods. Number of profiles used for the PCAP average profile = 4. Number of profiles used for the non-PCAP average profile = 7. Gray squares indicate that the species is not contributed by the source.

Optimized profiles for January 1 using the California seed

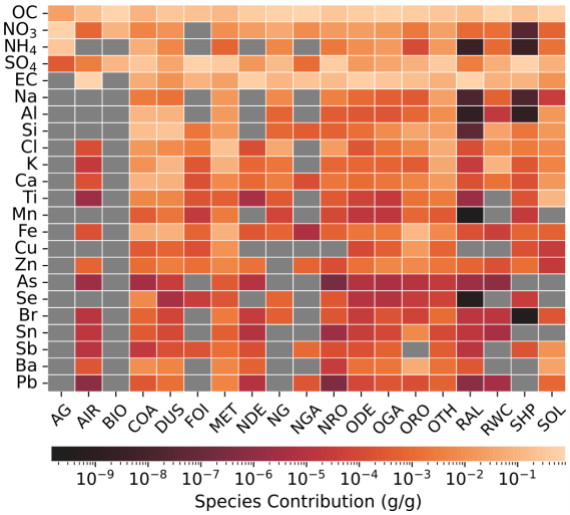

Figure S-33 Bakersfield CA ISAM profile.

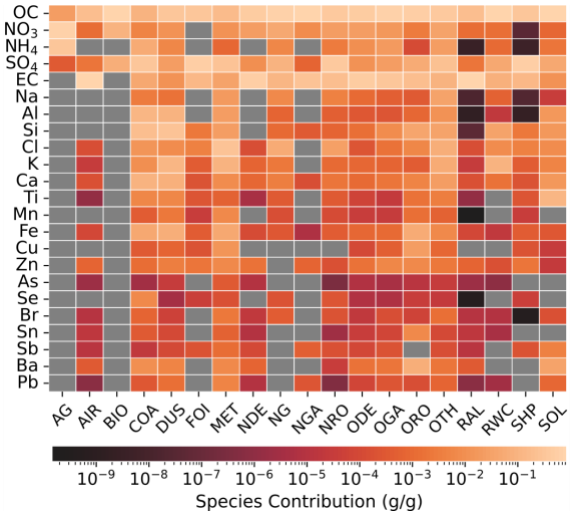

Figure S-34 Fresno CA ISAM profile.

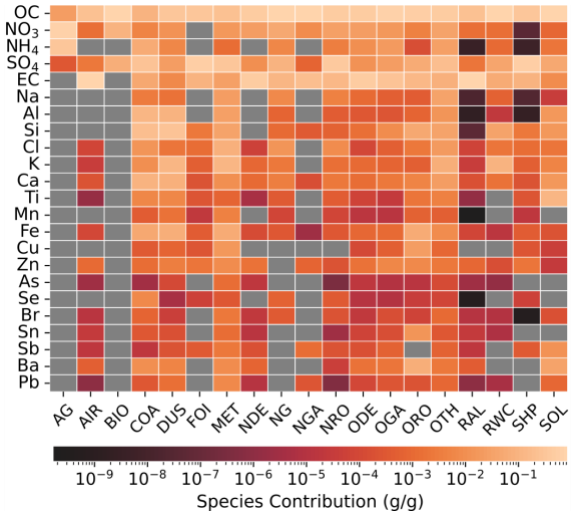

Figure S-35 Modesto CA ISAM profile.

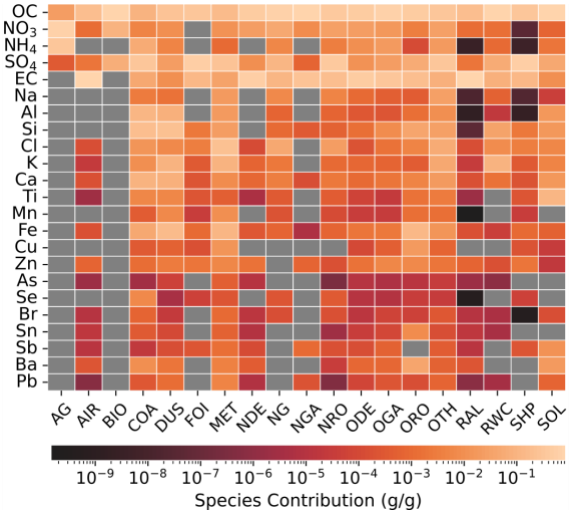

Figure S-36 Sacramento CA ISAM profile.

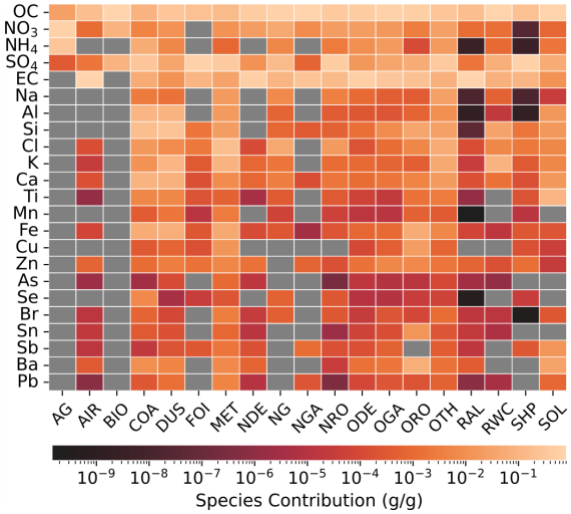

Figure S-37 Visalia CA ISAM profile.

References

(1) Ivey, C.; Holmes, H.; Shi, G.; Balachandran, S.; Hu, Y.; Russell, A. G. Development of PM $_{2.5}$ Source Profiles Using a Hybrid Chemical Transport-Receptor Modeling Approach. *Environ. Sci. Technol.* **2017**, *51* (23), 13788–13796. https://doi.org/10.1021/acs.est.7b03781.

(2) *Geographic Names Information System*. https://edits.nationalmap.gov/apps/gaz-domestic/public/gaz-record/1652668 (accessed 2025-03-27).

(3) *U.S. Census Bureau QuickFacts: Bakersfield city, California*. https://www.census.gov/quickfacts/fact/table/bakersfieldcitycalifornia/PST045224 (accessed 2025-03-17).